60 million years of ecological shifts in large herbivore communities revealed by Network Analysis

Fernando Blanco [a,b,c1], Ignacio A. Lazagabaster [c, d, e], Óscar Sanisidro [f], Faysal Bibi [c], Nicola S. Heckeberg [g,h], María Ríos [i], Bastien Mennecart [j], María Teresa Alberdi [k], Jose Luis Prado [l], Juha Saarinen [m], Daniele Silvestro [a,b,n], Johannes Müller [c], Joaquín Calatayud [o] & Juan L. Cantalapiedra [k]

[a] Department of Biological and Environmental Sciences, University of Gothenburg, Medicinaregatan 7B, 413 90 Gothenburg, Sweden.
[b] Gothenburg Global Biodiversity Centre, Box 463, 405 30 Gothenburg, Sweden.
[c] Museum für Naturkunde - Leibniz-Institut für Evolutions- und Biodiversitätsforschung, Invalidenstraße 43, 10549 Berlin, Germany.
[d] National Research Center on Human Evolution (CENIEH), Paseo Sierra de Atapuerca 3, 09002, Burgos, Spain.
[e] Department of Evolution, Ecology, and Behaviour, University of Liverpool, CH64 7TE, Liverpool, United Kingdom
[f] Universidad de Alcalá, GloCEE - Global Change Ecology and Evolution Research Group, Department of Life Sciences, 28805, Alcalá de Henares, Madrid, Spain.
[g] GeoBioCenter LMU, Ludwig-Maximilians-Universität München, Richard-Wagner-Str. 10, 80333 München, Germany.
[h] Department of Earth and Environmental Sciences, Palaeontology and Geobiology, Ludwig-Maximilians-Universität München, Richard-Wagner-Str. 10, 80333 München, Germany.
[i] Universidade Nova de Lisboa, 1099-085 Lisboa, Portugal.
[j] Naturhistorisches Museum Basel, Augustinergasse 2, CH – 4051 Basel, Switzerland.
[k] Museo Nacional de Ciencias Naturales (CSIC), José Gutiérrez Abascal 2, 28006 Madrid, Spain.
[l] Universidad Nacional del Centro de la Provincia de Buenos Aires. Del Valle 5737. B7400JWI-Olavarría, Argentina.
[m] Helsingin Yliopisto, Yliopistonkatu 4, 00100 Helsinki, Finland.
[n] Department of Biology, University of Fribourg and Swiss Institute of Bioinformatics, Ch. du Musée 10, 1700 Fribourg, Switzerland.
[o] Universidad Rey Juan Carlos, Calle Tulipán s/n, Móstoles, Spain.

*Fernando Blanco

Email: fblancosegovia@gmail.com

Author Contributions: F. Blanco and J.L.C. conceptualized the research. F. Blanco, I.A.L, O.S, F. Bibi, N.H, M.R, B.M., M.T.A., J.L.P, J.S. and J.L gathered the occurrence and trait data. F. Blanco, J.C., and J.L.C. designed and performed the analysis. F. Blanco and J.L.C. wrote the paper with input from all authors.

Keywords: Network analysis, macroecology, large herbivores, Cenozoic.

Abstract

The fossil record provides direct evidence for the behavior of biological systems over millions of years. In doing so, paleontological information becomes a key source to study the evolution of ecosystems and how they responded to major environmental shifts. Using network analysis over a dataset of worldwide large herbivores spanning the past 60 Myr, we found that large herbivore assemblages experienced long periods of ecological stability interrupted by irreversible reorganizations linked with abiotic events (tipping points). Initially, communities were characterized by mid-size browsers with low-crowned teeth and experienced increasing functional diversity until the formation of a land connection between Eurasia and Africa around 21 Ma. This was followed by a new functional system, the first tipping point, characterized by big-size browsers with mid to high crowned teeth. This new functional system experienced increasing functional diversity, with a peak ~10 Ma. It collapsed shortly thereafter, contemporaneous with global cooling and increased aridification that lead to the spread of C4-dominated grasslands, the second tipping point. It was replaced by a system characterized by a combination of grazers and browsers with high crowned teeth. Functional diversity has been decreasing since ~10 Ma, with an accelerated decline since ~2.5 Ma. Despite the diversity decline, the functional structure of terrestrial ungulate faunas has remained unaltered for the last part of the Cenozoic. The evolutionary history of large mammal assemblages is marked by two major functional transitions at critical points coincident with large-scale tectonic and climatic processes.

Introduction

The ongoing biotic crisis is characterized by a rapid deterioration of most Earth's ecosystems (1), which could be pushing several terrestrial and marine ecosystems towards new ecological regimes (functional "tipping points") (2-4). Such transitions, which are abrupt and irreversible over geological time, have been identified in the fossil record (5, 6), suggesting that past perturbations can be used as analogs to gain insights about the tempo and nature of immediate and future responses to environmental changes (7-9). Faunal shifts in the fossil record have been traditionally tackled from a taxonomic perspective (i.e., changes in taxonomic composition of communities and faunas; (10-13)). More recently, paleobiological studies have progressively incorporated taxon-free functional approaches, utilizing changes in ecomorphological composition to evaluate ecological shifts beyond taxonomic turnover (5, 14-16).

In terrestrial ecosystems, most of these functional approaches have focused on patterns of collapse of mammalian assemblages during the late Quaternary (14-16). A deeper temporal dimension is needed to provide a deeper understanding of the evolution of mammalian ecosystem dynamics and how they responded to major environmental shifts. Broadening the temporal scope should also reveal the mechanisms related to other patterns beyond collapse episodes, for example those involved in modulating ecological resilience and stasis (17), as well as processes underpinning dynamics of recovery and the unfolding of functional diversity. Because environmental change has a huge impact on ecosystem primary productivity and biomass transfer (18-20), investigating long-term patterns in primary consumer guilds should provide valuable insights into major ecological reconfigurations. Mammalian large herbivores have been the major vertebrate primary consumers in our planet's ecosystems in Cenozoic times. Ungulates consume disproportionately more plant biomass per unit area than any other vertebrate group (21). Many large mammalian herbivores are considered ecosystem engineers because they play a crucial role in processes involved in fire regimes control, seed dispersal, ecological succession of ecosystems, and soil compaction (21-27). Crucially, because of the recent and ongoing decline of large herbivores, these functions are largely missing from modern ecosystems. (26). In a search for a broader perspective on the behavior of terrestrial functional systems, we ask several questions: how did functional dynamics of terrestrial ecosystems shift over the Cenozoic? Are functional tipping points a common feature in these systems? Which factors triggered such ecological transitions?

Here, we aim to identify the main shifts in large herbivore functional structure of the orders Artiodactyla, Perissodactyla, and Proboscidea, which constitute most of the ungulate fossil record of the Cenozoic. As ecosystem engineers, terrestrial ungulates have a tight connection to physical changes and habitat disruptions, making them ideal to study current and past ecosystem functional transitions (21, 27). We developed an extensive database for large herbivores, containing occurrence information for 3,012 species spanning the past 60 million years. For each species, we gathered information for 14 ecomorphological traits (13 dental traits and body size) and clustered species based on their pairwise functional distances. We refer to these groups as 'functional types' (FT), since their constituent species would fulfill similar ecological roles. We then applied Network Analysis to identify ungulate continental assemblages with shared distributions of functional types, here called ungulate functional faunas (UFFs) (28). Therefore, these empirical faunas are unique associations of functional types that share specific patterns of geographical dynamics (i.e., they are highly interconnected in similar regions)(11, 29, 30). Our network analysis ignores assemblage age (is based exclusively on functional structure), and the temporal succession of UFFs is determined *a posteriori* (see methods). Lastly, we compared the results of our functional analyses with taxonomic faunas and the timing of major environmental shifts of the Cenozoic (31-34). Our results unveil two major shifts in the UFF succession coinciding with abiotic events.

Results and Discussion

Our results show a decoupling of taxonomic and functional assembly dynamics (Fig. 1A and Fig. S1). The functional structure of large herbivore assemblages exhibits greater resilience compared to their taxonomic structure. On average, taxonomic reassembly occurred every 1.7±0.31 Myr, whereas functional reconfiguration took place every 6.25±1.6 Myr. Sensitivity analyses validate these findings, ruling out potential artifacts stemming from sampling, aggregation or the selection of community detection algorithms (see methods and supplementary materials). Large herbivore assemblages experienced long periods of ecological stasis punctuated by two episodes of global functional reassembly (Fig. 1A). These tipping points occurred around 21 and 10 Ma, presumably as a response to major abiotic events. Since 10 Ma, large herbivore assemblages have experienced remarkable stability.

Early Cenozoic stability

For most of the Cenozoic, the faunas of America, Europe, and Asia were grouped under a single module representing a shared functional configuration (Fig. 1A) and occupied similar regions of functional space (Fig. 1B). Prior to 30 Ma, African faunas only had proboscideans among the orders examined here, so we are unable to assess the functional structure of this continent for this time period.

The Paleogene was a time dominated by mid-size browsers with low-crowned teeth (brachydont) (Figs. S4 and S17) of the families Paleotheriidae in Europe or Diacodexeidae in America (Fig. S18). Between 60 and 40 Ma, the system experienced a long period of functional stability (ecological stasis), with a reconfiguration in UFFs around 40 Ma, when American ungulate assemblages diverged functionally from those in Europe and Asia (Fig. 1A).

During the early Cenozoic, there is a global increase in functional diversity (Fig. 2). Functional diversity encapsulates both functional richness (the number of functional types) and functional evenness (the degree to which species are equally divided across functional types, see methods). Initially, this increase in functional diversity is primarily attributable to an increase in functional richness (Fig. 2) especially in American faunas, which exhibited a sustained increase in functional diversity between 50 and 20 Ma (Fig. 2B). In contrast, ungulate faunas of Europe and particularly Asia underwent a prolonged functional diversity decline during the early Cenozoic (Fig. 2). At about 40 Ma, these diverging trends culminated in the split of American ungulate assemblages from those in Europe and Asia (Fig. 1A and B). This functional reassembly coincided with the Middle Eocene Climatic Optimum (MECO, ca. 40.5 Ma) (34), a climatic disruption marked by a significant global temperature increase.

Europe and Asia formed a single UFF and shared a common functional trajectory until around ca. 32 Ma, when the European UFF diverged from the shared module with Asia (Fig. 1A). This divergence coincided with a period of global cooling that ultimately led to the formation of permanent ice sheets in Antarctica, marking the transition from the greenhouse climate of the Early Paleogene to the onset of the Late Cenozoic icehouse climate. This climatic shift, known as the Eocene-Oligocene transition (EOC), triggered major faunal extinctions and turnover in Europe, also dubbed as the *Grande Coupure* (35, 36), characterized by the influx of migrant faunas from Asia and replacing archaic ungulates with modern species (36, 37). Interestingly, the EOC caused less faunal disruption in Asia. Some families, such as Brontotheriidae, not only did not go extinct but diversified across the Asian continent during this period (35, 38). In contrast, the functional diversity of European faunas decreased, affected by the loss of functional richness (Fig. 1 and 2).

The African-Eurasian landbridge

The first global-scale reconfiguration of UFFs took place between 26 and 21 Ma, revealing a first tipping point. This period was marked by a homogenization of the functional structure of European, Asian, and African faunas (Fig. 1). The functional coalescence is reflected in the drastic reduction of the functional distance between Africa and Eurasia after 21 Ma (Fig. S3). A long process of environmental change, marked by a trend towards global aridification, began around 26 million years ago with the Alpino-Himalayan orogeny (39-41). This caused the collision of the African and Eurasian plates, which by 21 Ma resulted in the complete closure of the Tethys Sea, the emergence of the Mediterranean Sea, and the formation of a land connection known as the *Gomphotherium* landbridge (42).

The homogenization of faunas and the reassembly into a coherent, transcontinental UFF was therefore probably the result of the terrestrial connection between Eurasia and Africa at this time (Fig. 1A). This resulted in a net gain in functional diversity, with all three orders (Perissodactyla, Artiodactyla, Proboscidea) present across all three continents (Fig. 2). Notably, proboscideans dispersed out of Africa and spread around the world, triggering an acceleration of ecomorphological evolution within this order (43). However, the impact of the *Gomphotherium* landbridge worked in both directions. Artiodactyls and perissodactyls, which had dominated the large herbivore fauna in Eurasia since the beginning of the Cenozoic, dispersed into Africa, exploiting different niches within the functional space (Fig. 1B). Simultaneously, the Americas underwent a reassembly of their functional assemblage, characterized by mid-size grazers with medium to high crowned teeth. However, the Americas continued to follow their distinct trajectory, remaining unique and isolated from the rest of the continents in terms of functional structure (Fig. 1A). Subsequent to this event, the Americas' UFF started an opposite trend towards Eurasia, experiencing a continuous decline in diversity (Fig. 2B). Such declines eventually manifested also in other parts of the world (Fig. 2B). Overall, the onset of the tectonic movements that lead to the formation of the *Gomphotherium* landbridge created new ecological configurations, marking a milestone event in the evolutionary history of terrestrial mammal faunas.

The global expansion of grasslands

Emerging from a continuous trend of increasing functional diversity, mainly driven by a rise in functional richness (Fig. 2), the functional network appears to have reached a second global tipping point ca. 10 Ma (34, 44). From this moment, there was a drop in global functional diversity that has persisted to the present day (Fig. 2). A decline that resulted in the loss of 65% of functional diversity in less than 5 Myr (from 10 to 5 Ma, see Fig. 2). This trend prompted a contemporaneous reassembly of UFFs across continents, characterized by a combination of grazers and browsers with high crowned teeth (Fig. S4, S5 and S17). This reassembly was first observed in African faunas, resulting in their divergence from the previous module shared with Eurasian faunas (Fig. 1). European faunas, followed by the faunas of the Americas and Asia, also underwent a reorganization of their functional structure similar to Africa's (Fig. 1A). This reconfiguration made European and Asian functional assemblages to shortly diverge from each other for two million years (Fig. 1A and S3). After around 4.5 Ma, the ungulate faunas of both

continents would fall back under the same functional configuration, a coherent structure that lasted until current days (Fig. 1A).

Humid-like forested environments had dominated the world's ecosystems prior to the Middle Miocene Climatic Optimum (45), but after this event the world transitioned towards a drier and colder climate (34). These conditions favored the expansion of C4-dominated grasslands and the development of morphological adaptations to these new environments (46-48). Herbivores had to adapt their dentition to cope with the high abrasion imposed by the new vegetation: increase of tooth height (hypsodonty), thicker enamel, or larger molar occlusal areas (49-52). Consequently, new functionalities emerged as ecological opportunities diversified, shaping the exploration of different regions within the functional space (Fig. 1B). The novel environmental settings provided ideal conditions for certain groups to diversify (e.g. Equids, (53)), while the decline of forest-humid environments worldwide triggered a drastic decrease in global functional diversity (43) (Fig. 2). The decline of the functional diversity that started 10 Ma has continued unmatched until the present.

The Quaternary and the functional configuration of modern faunal assemblages

The persistent trend of declining global functional diversity, which commenced ca. 10 Ma, underwent acceleration ca. 2.5 Ma (Fig. 2). Segmented regression analysis (see methods) indicated a significant drop in global functional diversity, a trend that continued until the present day (Fig. 2). The last part of the Cenozoic was characterized by increasingly arid and cold environments (34). This trend started 10 Ma, after the MMCO, but around 5 Ma the onset of the Plio-Pleistocene glaciations increased these environmental conditions (34, 54, 55).

Our findings provide a broad ecological perspective for the demise of large herbivores, exemplified by the iconic megafauna. During the last part of the Cenozoic the decline of large herbivores started, marking a prolonged trend of decline in these faunas (43, 56, 57). This functional attrition is better exemplified by the Proboscideans, a successful group of large herbivores with a peak of 33 species coexisting ca. 3.2 Ma, immediately before the intensification of the Plio-Pleistocene glaciations, which initiated their decline (43). However, the functional collapse also affected artiodactyls and perissodactyls, as evidenced by the acceleration in the global decline of functional diversity (Fig. 2).

Once again, an opposite trend in functional diversity is recorded in America. As other continents witnessed a demise of their functional diversity, American ungulate faunas underwent a minor recovery of functional diversity resulting from an increase in functional evenness (Fig. 2A and B). We suggest that, as with the formation of the *Gomphotherium* landbridge, the formation of a natural corridor between North and South America was responsible for this rebounding in functional diversity. Around 2.6 Ma, the Panama isthmus formed (58, 59), triggering the Great American Biotic Interchange (60-63). New opportunities appeared in the niches from both continents, triggering exploration into new regions of the functional space (Fig. 1B) (62, 64). The colonization of novel environments by large herbivore groups found across both continents has led to an increase in their functional diversity. This is primarily due to an increase in evenness, meaning that species are more uniformly spread across different functional roles within the ecosystems of North and South America. (Fig. 2B).

However, these changes in functional diversity do not appear to significantly alter the essential functional scaffold of large herbivore continental functional pools (Fig. 1A). From 4.5 Ma, UFFs remained globally unaltered, representing a functional structure stasis that persists to the present day. This stasis has endured even through periods of major abiotic crisis, such as the Messinian Salinity Crisis or the Plio-Pleistocene glaciations, which appear to have affected the functional diversity (Fig. 2). Unlike in past events, the system is resilient enough to overcome the sustained loss of functional diversity and remains unaffected in its essential functional configuration (Fig. 1A and Fig. 2). The UFFs could overcome the tremendous species loss thanks to their ecological interactions (insurance effect)

(65), where a taxon could be extinct, but its ecological role can be performed by others, preserving the functional structure of the system (Fig. 1).

Interestingly, our results do not seem to reflect the recent loss of megafauna on the UFFs (Fig. 1). The extinction of these species became more prominent after the Late Pleistocene, with most of the forms becoming extinct except for a few species that remain in our terrestrial ecosystems today (26). Due to this extinction, large herbivore communities and the ecosystems they inhabit have drastically changed over the last 129 kyr (26, 66-68). However, by the end of the Cenozoic (from 129 kyr to the present), these species represented only 18% of the total FTs of large herbivore assemblages (Fig. S22 and S23), comprising a small part of the composition of these assemblages at a continental scale. Moreover, 81% of the FTs in the last 11.700 years remain on all continents even after the loss of megafauna-composed FTs (Fig. S22 and S23). Despite the loss of the megafauna, the functional configuration of the large herbivore assemblages has been preserved in terms of UFFs over the last 4.5 Myr (modules 7,8 and 9 in Fig. 1). Our results yield a cautionary reading because the vague connection between the taxonomic and functional assembly does not directly reflect the loss of the megafauna in terrestrial ecosystems. These species performed functions in terrestrial ecosystems that are largely missing due to their extinction. Conservation efforts to preserve or reintroduce (69-71) these species in terrestrial ecosystems become mandatory to restore the functioning of our world ecosystems today.

Conclusions

Our study portrays a dynamic functional system within large herbivore assemblages throughout the Cenozoic, characterized by periods of ecological stability and reassembly. Over broad temporal and spatial scales, large herbivores' functional dynamics appear mainly driven by major abiotic changes. Such events pushed the system beyond points of no-return (tipping points), forcing the reassembly into new stable states. We found two major moments of functional reassembly of terrestrial ungulate faunas that occurred synchronously across all continents. During these events, large herbivore functional structure followed analogous trajectories in the functional space at the continental level, displaying recurrent functional homogeneity following reassembly events.

Our results show that functional systems could be resilient enough to overcome the loss of ecological roles, maintaining their functional essence during moments of environmental change. Over the last 4.5 million years, large herbivore assemblages experienced a long period of functional structure stability, overcoming even several abiotic crises, which has lasted until the present. However, this period was characterized by an unchecked decline in the functional diversity of these groups, resulting in an impoverishment of large herbivore ecosystems. If prolonged and worsened by current human aggressions to the environment, we do not know when this functional impoverishment will irreversibly affect the essential pillars of the large herbivore continental functional pool. This could potentially lead to the next tipping point and functional reassembly of the system.

Material and Methods

Database

We built a database for all the species in the largest orders of large herbivores living in earth current ecosystems (Artiodactyla, Perissodactyla, and Proboscidea) during the last 60 Ma. First, we compiled information for these species through a review of the primary literature along with data available in the NOW database and the Paleobiology Database (PBDB) (72, 73). Second, following (74) each species occurrence was checked in detail by experts in their taxonomic groups, looking for valid taxonomic assignments and excluding synonyms. Only records identified at the species level were retained. Third, we used the *International Chronostratigraphic Chart* (75) to build a consistent scheme for temporal ranges across our dataset. We checked each record in order to improve their temporal resolution through a deep survey of the literature. In some cases, there were occurrences with a broad temporal range assigned (i.e., old publications of sites with scarce stratigraphic information, early sites with a

wide range of temporal assignment, or incorrect entries in the databases). When we could not find better age ranges in the literature we excluded these records from our database. We decided to exclude the occurrences with a temporal range exceeding 5 Myr in the Neogene and 10 Myr in the Paleogene. For the Plio-Pleistocene records, we manually selected the ones with broad ranges and improved them using the most recent literature.

Since we used a combination of NOW and PBDB data, we obtained duplicated records for the species in our dataset. We chose between these records based on manual, case-by-case evaluation criteria of occurrence number and overall occurrence temporal precision. As a result, after all our criteria and review procedure was applied, we obtained a final dataset that contains 22,028 occurrences of 3,046 species distributed in 10,680 sites worldwide.

Our aim was to characterize the succession of functional assemblages over evolutionary time scales. To do so, we gathered information for 13 dental traits and body size for the species in our dataset. Based on (76), we compiled dental trait information for: tooth shape, degree of hypsodonty, cusp shape, number of buccal cusps, number of lingual cusps, number of longitudinal lophs, number of transverse lophs, horizodonty, as well as the presence of acute lophs, obtuse lophs, structural fortification cusps, occlusal topography, and coronal cementum (see Žliobaitė*, et al.* (76), Fortelius*, et al.* (77), Zliobaite*, et al.* (78) for a detailed description of these traits). These dental traits are fundamental because they capture the relationship of the species with environmental conditions, especially being a good predictor of net primary production or precipitation (76). Besides, we classified species in eight body size categories modified from (79, 80): B (<1kg), C (1-10kg), D (10-45kg), E (45-90kg), F (90-180kg), G (180-360kg), H (360-1,000kg), I (1,000-10,000kg) and J (>10,000kg). We excluded the original category A (0-0.1kg), because we did not have species in this body size range in our database. Overall, these traits reflect several facets of the functional role of species in ecosystems, such as habitat use, trophic level, range size, energetic requirements, and resource use (10, 81).

Spatio-temporal standardization

Working with large databases in paleontology has some difficulties, especially regarding the duplication or wrong assignment of locality' names and the heterogeneity of stratigraphic ages. In order to prevent this, when we built our occurrence matrix, we merged the localities using two criteria. First, we aggregated the localities by continent (Africa, America, Asia, and Europe). To characterize macroevolutionary dynamics of Cenozoic faunas, a continental scale allowed us to track changes worldwide and check the correlation of these changes with crucial abiotic shifts in Earth' history such as plate tectonics or climate change. Second, we aggregated localities into temporal stages defined by the *International Chronostratigraphic Chart* stages (66, 61.6, 59.2, 56, 47.8, 41.2, 37.71, 33.9, 27.82, 23.03, 20.44, 15.97, 13.82, 11.63, 7.246, 5.333, 3.6, 2.58, 1.8, 0.774, 0.129 and 0.0117 Myr). The aggregation of localities by continent and stage yielded a total of 78 continent-stage assemblages, which are the analytical basis for the study. The use of continent-stage pools helped to avoid potential errors in the age assignments of the fossil localities.

Characterization of ungulate function faunas

Since we consider body size and tooth shape fundamental traits to define the species' role in the ecosystems, we excluded the species with no information about these traits (this was the case for only 34 species). The final dataset contained functional information for 3,012 species, which formed the basis for all the analysis. To study the role of these species in their ecosystems, we had to reduce the dimensionality of our large mammal trait dataset. We computed Gower distances between species trait dataset using the *daysy* function in *R* (82). During the computation of functional distances between species, each trait was given a different importance, so that dental traits would not have a disproportional weight in the total difference among species. To do so, we weighted two of the traits to 1 (body size and tooth shape), because they were the most representative traits of the species' relationship with their environment, and assigned a weight of 1 / 6 to the remaining 12 traits (hypsodonty,

cusp shape, buccal cusps, lingual cusps, longitudinal lophs, transverse lophs, horizodonty, acute lophs, obtuse lophs, structural fortification cusps, occlusal topography, and coronal cementum), thus summing up to 2, which is the result of the other traits combined.

We used the resulting distance matrix in a Principal Coordinates Analysis (PCoA). Based on the functional morphospace obtained from the PCoA, we applied a *k-means* to define groups of species with similar ecological roles: functional types (FT). Species closer in the functional morphospace will be grouped in the same FT. We decided on a maximum of 406 FTs, which was the number of unique combinations of the traits in our dataset (also called functional entities Mouillot*, et al.* (83)).

Our approach resulted in a final dataset with 406 FT distributed along 78 continent-stage pools, which were the basis for our analysis.

Network analysis

Following Blanco*, et al.* (5), we used the developed Network Analysis approach to track the dynamics in the ecological assembly of large mammal continental functional pool worldwide over the last 65 Myr.

Input data. To explore the temporal organization of functional and taxonomical assemblages, we applied a community detection procedure borrowed from network theory (84, 85). This analysis finds groups of localities sharing similar functional types (or taxa) regardless of the temporal sequence, allowing us to delve into the functional evolution of assemblages. We first transformed the fossil occurrence data into bipartite networks. Bipartite networks consist of two different sets of nodes that are not mutually connected. In our case, these two sets of nodes were continent-stage and functional types (or taxa). A link depicted the presence of a functional type (or taxa) in a continental bin. Moreover, for the functional network we weighted the links as the number of species belonging to a functional type and present in a continental bin. By doing so, we quantified the relative importance of each functional type in a continental bin.

Community detection algorithm. Once we generated the networks, we ran the *Infomap* community detection algorithm (86, 87), to find network communities or modules. As explained above, these modules represent groups of localities sharing functional types (or taxa), which are, in turn, mostly distributed within the localities. That is to say, *Infomap* provides a simultaneous classification of continent-stage and functional types (or taxa) (88). *Infomap* capitalizes on the minimum description length principle of information theory, which equates finding regularities and compression: the model that finds most regularities in a given set of data can compress the data the most (89). In our case, modules of highly interconnected continent-stage and functional types (or taxa) form the regularities, and describing the network with an optimal set of assemblages corresponds to minimizing the description length (87, 88). *Infomap* minimizes the description length using a heuristic algorithm where nodes are stochastically placed into modules and movements are accepted if the description length reduces. We used this algorithm because it performs better than other community detection methods (88, 90). We ran *Infomap* 10,000 times, selecting the best partition as measured by the description or code length (87). This number of runs provided a complete solution landscape. Moreover, modules were consistent across runs and alternative community detection algorithms (see Sensitivity analysis to community detection).

We plotted the resulting modules through time for the taxonomic and functional types configuration (Fig. 1 and S1).

Functional space

Beta diversity. In order to track the functional evolution of large herbivores, we calculated the difference in functional diversity between the different continent-stage. To do so, we used the *betapart* package in *R* (91). This package calculates multi-sites distances using pairwise dissimilarities (in our case using

as a basis the distance matrix between species in each bin). The advantage of using this package is that it allows to calculate the turnover and nestedness, components of functional beta diversity. Here, we used turnover as the difference of functional types composition between continent-stages, and nestedness when functional types assemblages in functional type-poor continent-stage are a subset of the assemblages in more functional type-rich continent-stage. We ran the *functional.beta.pair* function, which computes functional dissimilarities based on volume of convex hull intersections in a multidimensional functional space. Dissimilarity matrix accounting for functional turnover, was measured as Simpson derived pairwise functional dissimilarity, nestedness-resultant functional dissimilarity and functional beta diversity, was measured as the nestedness-fraction and beta diversity of Sorensen derived pair-wise functional dissimilarity. We plotted the change in these three measures over time, calculating the change from the previous temporal bin for each continent (Fig. S2).

We applied a non-metric multidimensional scaling (NMDS) to reduce the dissimilarity variability in two axes to plot the functional trajectories of continental assemblages over time in two dimensions. In this case, we decided to use the turnover distance matrix for the main part of the discussion and figures, as our interest is to track the functional change over time, which is the key information in order to study the dynamics of these faunas. We plotted the results using a temporal color-scale and module scale colors, obtained from the network analysis, for each continent (Fig. 1B).

Functional diversity

Once we characterized the functional structure and their evolution using network analysis (see above), we looked into the changes of functional diversity. This allows us to study the patterns that affect the functional diversity of these faunas and compare them with the dynamics of functional structure assembly. To do so, we calculated the functional diversity for all the temporal bins separated by each continent (continent-stage) in our database. We computed this for each continent-stage based only on the functional types (i.e. groups of species with similar ecological roles, see above) belonging to the same module, from network analysis, as the continental bin.

We first use the Shannon's diversity index, which considers both the richness of functional types and even distribution of species into functional types:

$H = -\sum^{R}_{i=1} pi\ ln(pi)$ (Eq. 1)

where *R*, is the number of functional types (also referred here as functional richness), and *pi* is the proportion of species belonging to the *i* functional type. High values of the Shannon index indicate high continental functional richness (number of functional types) and a more homogeneous distribution of species along the functional types found in a particular continent-stage. Thus, high Shannon values indicate high values of ecological disparity (high number of functional types) coupled with high values of ecological redundancy (species evenly distributed along the functional types).

Then, we also considered each constituent part of the Shannon index (i.e. richness and evenness) independently. To measure evenness, we used the Pielou's index, calculated as,

$J=H/ln(R)$ (Eq.2)

where H' comes from Shannon's diversity index. High values of evenness indicate high ecological redundancy, which means that species tend to be evenly spread across functional types (i.e. ecological roles).

For the calculation of these indexes we used only continent-stage assemblages with more than 20 species, following the sensitivity analysis to sampling performed (see supplementary).

We used *R* software (82) for all the analyses. All the scripts and database used are at: https://github.com/f-blanco/ecoherb

Acknowledgements

We thank M. Hernández Fernández, P. Medina-García, I. Menéndez, G. Navalón and the Amniota lab for their valuable comments and advice. Fernando Blanco was funded by the Deutsche Forschungsgemeinschaft (Projektnummer: 351155510) and by Gothenburg University via the Swedish Research Council (VR: 2019-04739). We acknowledge the effort of all the people working in fossil sites over the decades that made this study possible.

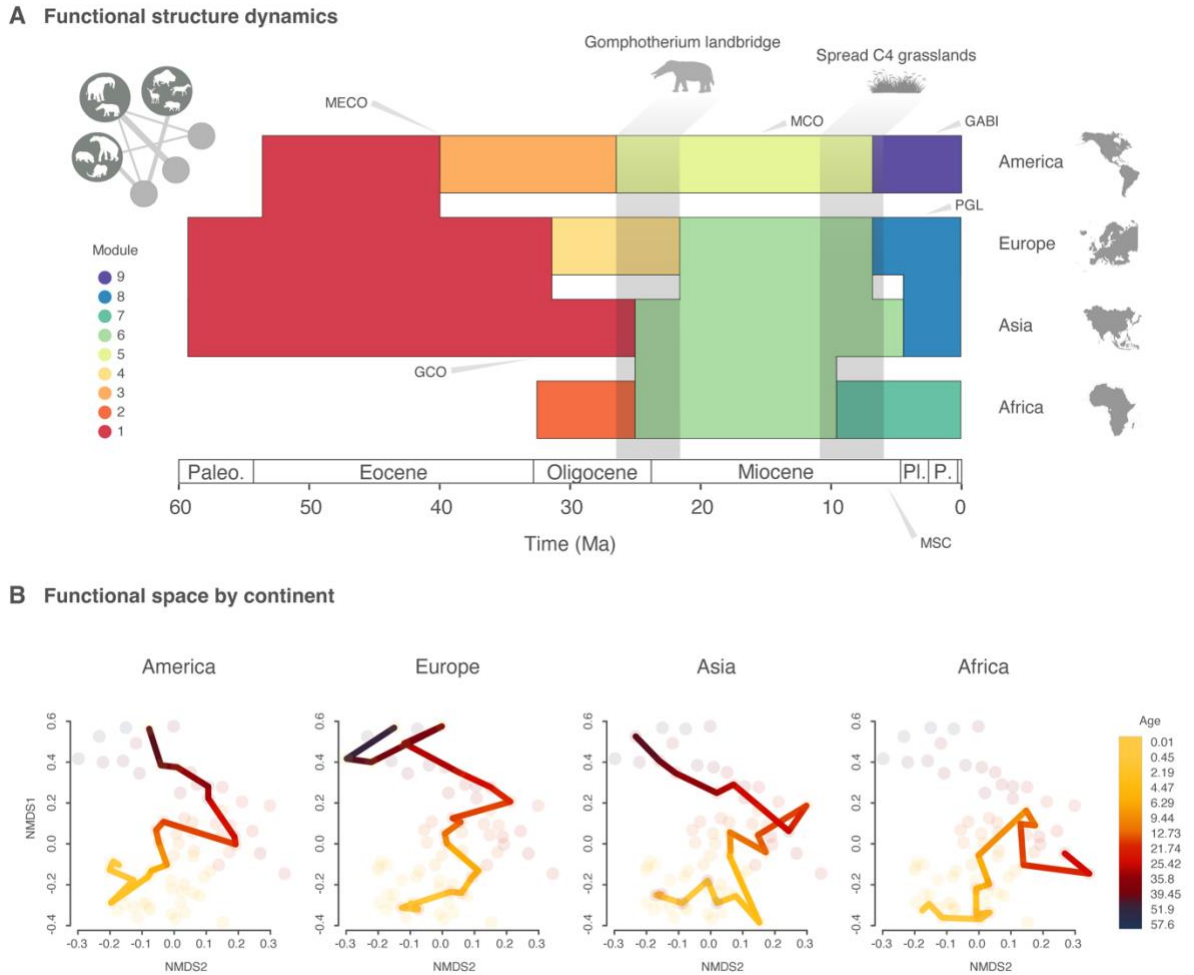

Fig. 1. Cenozoic dynamics of large herbivore functional structure. (A) The nine main functional modules plotted across time and by continent. Note distinct differences between Paleogene and Neogene modules, and also shared modules across Africa and Eurasia, and the long-term distinctiveness of the American continents. Since the African dataset prior to 34 Ma only includes proboscideans, we decided to exclude it from the analysis. Abbreviations: Paleo., Paleocene, Pl., Pleiocene, P., Pleistocene, MECO, Middle Eocene Climatic Optimum, GCO, Grande Coupure, MCO, Middle Miocene Climatic Optimum, MSC, Messinian Salinity Crisis, PGL, Plio-Pleistocene Glaciations, GABI, Great American Biotic Interchange. (B) Functional space for each continent plotted using non-metric multidimensional scaling (NMDS). Dots represent time bins in each continent. The line of best fit shows functional changes across time. Silhouettes are from phylopic.org.

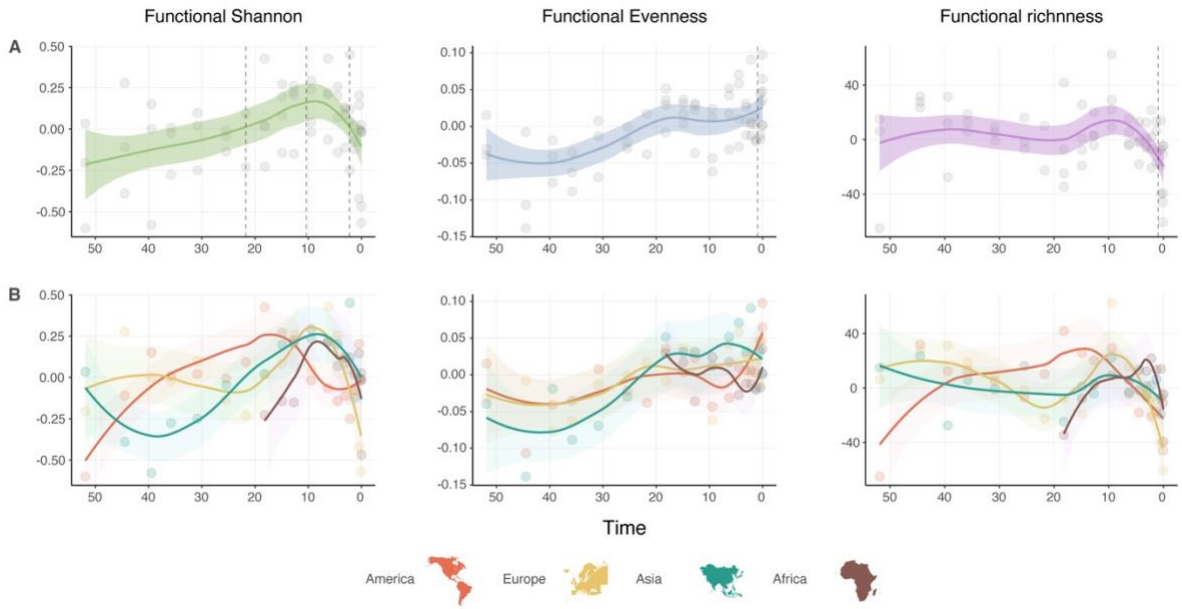

Fig. 2. Functional diversity dynamics of large herbivores. Residuals of diversity indexes (Shannon index, evenness index, and functional richness) are plotted against time in Myr (see supplementary methods), (A) showing total values and (B) divided by continents. Curves are derived from a local regression fitting (LOESS). Shaded areas represent the 95% confidence interval of LOESS fit. Dotted lines are inflection points from regression models with segmented relationships (see methods).

References

1. V. Masson-Delmotte, P. Zhai, A. Pirani, S.L. Connors, C. Péan, S. Berger, N. Caud, Y. Chen, L. Goldfarb, M.I. Gomis, M. Huang, K. Leitzell, E. Lonnoy, J.B.R. Matthews, T.K. Maycock, T. Waterfield, O. Yelekçi, R. Yu, and B. Zhou (eds.) (2021) IPCC, 2021: Climate Change 2021: The Physical Science Basis. Contribution of Working Group I to the Sixth Assessment Report of the Intergovernmental Panel on Climate Change. (Cambridge University Press).
2. A. D. Barnosky *et al.*, Merging paleobiology with conservation biology to guide the future of terrestrial ecosystems. *Science* **355**, eaah4787 (2017).
3. C. H. Trisos, C. Merow, A. L. Pigot, The projected timing of abrupt ecological disruption from climate change. *Nature* **580**, 496-501 (2020).
4. D. I. Armstrong McKay *et al.*, Exceeding 1.5 C global warming could trigger multiple climate tipping points. *Science* **377**, eabn7950 (2022).
5. F. Blanco *et al.*, Punctuated ecological equilibrium in mammal communities over evolutionary time scales. *Science* **372**, 300-303 (2021).
6. Y. Huang *et al.*, The stability and collapse of marine ecosystems during the Permian-Triassic mass extinction. *Current Biology* **33**, 1059-1070. e1054 (2023).
7. C. Pimiento, A. Antonelli, Integrating deep-time palaeontology in conservation prioritisation. *Frontiers in Ecology and Evolution* **10**, 959364 (2022).
8. C. Pimiento *et al.*, The Pliocene marine megafauna extinction and its impact on functional diversity. *Nature ecology & evolution* **1**, 1100-1106 (2017).
9. C. Pimiento *et al.*, The extinct marine megafauna of the Phanerozoic. *Cambridge Prisms: Extinction* **2**, e7 (2024).
10. B. Figueirido, C. M. Janis, J. A. Pérez-Claros, M. De Renzi, P. Palmqvist, Cenozoic climate change influences mammalian evolutionary dynamics. *Proceedings of the National Academy of Sciences* **109**, 722-727 (2012).
11. B. Figueirido, P. Palmqvist, J. A. Pérez-Claros, C. M. Janis, Sixty-six million years along the road of mammalian ecomorphological specialization. *Proceedings of the National Academy of Sciences* **116**, 12698-12703 (2019).
12. R. K. Bambach, J. B. Bennington, Do communities evolve? A major question in evolutionary paleoecology. *Evolutionary Paleobiology: University of Chicago Press, Chicago*, 123-160 (1996).

13. J. M. Pandolfi, T. L. Staples, W. Kiessling, Increased extinction in the emergence of novel ecological communities. *Science* **370**, 220-222 (2020).
14. F. A. Smith *et al.*, Late Pleistocene megafauna extinction leads to missing pieces of ecological space in a North American mammal community. *Proceedings of the National Academy of Sciences* **119**, e2115015119 (2022).
15. D. Fraser *et al.*, Late quaternary biotic homogenization of North American mammalian faunas. *Nature Communications* **13**, 3940 (2022).
16. C. P. Hedberg, S. K. Lyons, F. A. Smith, The hidden legacy of megafaunal extinction: Loss of functional diversity and resilience over the Late Quaternary at Hall's Cave. *Global Ecology and Biogeography* **31**, 294-307 (2022).
17. P. D. Roopnarine, R. M. Banker, Ecological stasis on geological time scales. *Science* **372**, 237-238 (2021).
18. J. M. Melillo *et al.*, Global climate change and terrestrial net primary production. *Nature* **363**, 234-240 (1993).
19. J. L. Blanchard *et al.*, Potential consequences of climate change for primary production and fish production in large marine ecosystems. *Philosophical Transactions of the Royal Society B: Biological Sciences* **367**, 2979-2989 (2012).
20. F. Bibi, J. L. Cantalapiedra, Plio-Pleistocene African megaherbivore losses associated with community biomass restructuring. *Science* **380**, 1076-1080 (2023).
21. W. J. Ripple *et al.*, Collapse of the world's largest herbivores. *Science advances* **1**, e1400103 (2015).
22. J. Brits, M. Van Rooyen, N. Van Rooyen, Ecological impact of large herbivores on the woody vegetation at selected watering points on the eastern basaltic soils in the Kruger National Park. *African Journal of Ecology* **40**, 53-60 (2002).
23. C. van der Waal *et al.*, Large herbivores may alter vegetation structure of semi-arid savannas through soil nutrient mediation. *Oecologia* **165**, 1095-1107 (2011).
24. R. van Klink, J. van Laar-Wiersma, O. Vorst, C. Smit, Rewilding with large herbivores: Positive direct and delayed effects of carrion on plant and arthropod communities. *PloS one* **15**, e0226946 (2020).
25. A. T. Karp, A. K. Behrensmeyer, K. H. Freeman, Grassland fire ecology has roots in the late Miocene. *Proceedings of the National Academy of Sciences* **115**, 12130-12135 (2018).
26. F. A. Smith, C. E. Doughty, Y. Malhi, J. C. Svenning, J. Terborgh (2016) Megafauna in the Earth system. (Wiley Online Library), pp 99-108.
27. J. Trepel *et al.*, Meta-analysis shows that wild large herbivores shape ecosystem properties and promote spatial heterogeneity. *Nature Ecology & Evolution* **8**, 705-716 (2024).
28. F. Blanco *et al.*, Punctuated ecological equilibrium in mammal communities over evolutionary timescales (Code).
29. J. J. Sepkoski, R. K. Bambach, D. M. Raup, J. W. Valentine, Phanerozoic marine diversity and the fossil record. *Nature* **293**, 435-437 (1981).
30. K. Flessa, J. Imbrie, D. Tarling, S. Runcorn, Implications of continental drift to the earth sciences. (1973).
31. S. Lamb, P. Davis, Cenozoic climate change as a possible cause for the rise of the Andes. *Nature* **425**, 792-797 (2003).
32. M. Mudelsee, T. Bickert, C. H. Lear, G. Lohmann, Cenozoic climate changes: A review based on time series analysis of marine benthic δ18O records. *Reviews of Geophysics* **52**, 333-374 (2014).
33. D. E. Billings *et al.* (1968) Cenozoic climatic change and its cause. in *Causes of climatic change: a collection of papers derived from the INQUA—NCAR symposium on causes of climatic change, August 30–31, 1965, Boulder, Colorado* (Springer), pp 128-133.
34. T. Westerhold *et al.*, An astronomically dated record of Earth's climate and its predictability over the last 66 million years. *Science* **369**, 1383-1387 (2020).
35. D. R. Prothero, W. A. Berggren, *Eocene-Oligocene climatic and biotic evolution* (Princeton University Press, 2014), vol. 135.
36. R. Weppe, F. L. Condamine, G. Guinot, J. Maugoust, M. J. Orliac, Drivers of the artiodactyl turnover in insular western Europe at the Eocene–Oligocene Transition. *Proceedings of the National Academy of Sciences* **120**, e2309945120 (2023).
37. S. Legendre (1987) Les immigrations de la «Grande Coupure» sont-elles contemporaines en Europe occidentale. in *International Symposium on Mammalian Biostratigraphy and Paleoecology of the European Paleogene, Mainz. Münchner Geowissenschaftliche Abhandlungen A*, pp 141-147.

38. O. Sanisidro, M. C. Mihlbachler, J. L. Cantalapiedra, A macroevolutionary pathway to megaherbivory. *Science* **380**, 616-618 (2023).
39. S. K. Mandal *et al.*, Multiproxy isotopic and geochemical analysis of the Siwalik sediments in NW India: Implication for the late Cenozoic tectonic evolution of the Himalaya. *Tectonics* **38**, 120-143 (2019).
40. J. Mey *et al.*, Glacial isostatic uplift of the European Alps. *Nature Communications* **7**, 13382 (2016).
41. M. Harzhauser *et al.*, Biogeographic responses to geodynamics: a key study all around the Oligo–Miocene Tethyan Seaway. *Zoologischer Anzeiger-A Journal of Comparative Zoology* **246**, 241-256 (2007).
42. O. M. Bialik, M. Frank, C. Betzler, R. Zammit, N. D. Waldmann, Two-step closure of the Miocene Indian Ocean Gateway to the Mediterranean. *Scientific Reports* **9**, 1-10 (2019).
43. J. L. Cantalapiedra *et al.*, The rise and fall of proboscidean ecological diversity. *Nature Ecology & Evolution* **5**, 1266-1272 (2021).
44. C. P. Chamberlain, M. J. Winnick, H. T. Mix, S. D. Chamberlain, K. Maher, The impact of Neogene grassland expansion and aridification on the isotopic composition of continental precipitation. *Global Biogeochemical Cycles* **28**, 992-1004 (2014).
45. W. J. Bond, What limits trees in C4 grasslands and savannas? *Annual review of ecology, evolution, and systematics* **39**, 641-659 (2008).
46. E. J. Edwards *et al.*, The origins of C4 grasslands: integrating evolutionary and ecosystem science. *science* **328**, 587-591 (2010).
47. C. A. Strömberg, F. A. McInerney, The Neogene transition from C3 to C4 grasslands in North America: assemblage analysis of fossil phytoliths. *Paleobiology* **37**, 50-71 (2011).
48. J. T. Faith, J. Rowan, A. Du, Late Cenozoic Faunal and Ecological Change in Africa. *Annual Review of Earth and Planetary Sciences* **52** (2024).
49. C. M. Janis, M. Fortelius, On the means whereby mammals achieve increased functional durability of their dentitions, with special reference to limiting factors. *Biological Reviews* **63**, 197-230 (1988).
50. J. Jernvall, M. Fortelius, Common mammals drive the evolutionary increase of hypsodonty in the Neogene. *Nature* **417**, 538-540 (2002).
51. P. Lucas, P. Constantino, B. Wood, B. Lawn, Dental enamel as a dietary indicator in mammals. *BioEssays* **30**, 374-385 (2008).
52. P. S. Ungar, Mammalian dental function and wear: a review. *Biosurface and Biotribology* **1**, 25-41 (2015).
53. J. L. Cantalapiedra, J. L. Prado, M. Hernández Fernández, M. T. Alberdi, Decoupled ecomorphological evolution and diversification in Neogene-Quaternary horses. *Science* **355**, 627-630 (2017).
54. W. F. Ruddiman, A paleoclimatic enigma? *Science* **328**, 838-839 (2010).
55. G. Kukla, V. Cílek, Plio-Pleistocene megacycles: record of climate and tectonics. *Palaeogeography, Palaeoclimatology, Palaeoecology* **120**, 171-194 (1996).
56. F. A. Smith, R. E. Elliott Smith, S. K. Lyons, J. L. Payne, Body size downgrading of mammals over the late Quaternary. *Science* **360**, 310-313 (2018).
57. F. A. Smith, R. E. E. Smith, S. K. Lyons, J. L. Payne, A. Villaseñor, The accelerating influence of humans on mammalian macroecological patterns over the late Quaternary. *Quaternary Science Reviews* **211**, 1-16 (2019).
58. A. O'Dea *et al.*, Formation of the Isthmus of Panama. *Science advances* **2**, e1600883 (2016).
59. C. D. Bacon *et al.*, Biological evidence supports an early and complex emergence of the Isthmus of Panama. *Proceedings of the National Academy of Sciences* **112**, 6110-6115 (2015).
60. F. G. Stehli, S. D. Webb, *The great American biotic interchange* (Springer Science & Business Media, 2013), vol. 4.
61. M. O. Woodburne, The Great American Biotic Interchange: dispersals, tectonics, climate, sea level and holding pens. *Journal of mammalian evolution* **17**, 245-264 (2010).
62. L. Domingo, R. L. Tomassini, C. I. Montalvo, D. Sanz-Pérez, M. T. Alberdi, The Great American Biotic Interchange revisited: a new perspective from the stable isotope record of Argentine Pampas fossil mammals. *Scientific reports* **10**, 1-10 (2020).
63. J. D. Carrillo *et al.*, Disproportionate extinction of South American mammals drove the asymmetry of the Great American Biotic Interchange. *Proceedings of the National Academy of Sciences* **117**, 26281-26287 (2020).
64. S. D. Webb, "Late Cenozoic mammal dispersals between the Americas" in The great American biotic interchange. (Springer, 1985), pp. 357-386.

65. S. Yachi, M. Loreau, Biodiversity and ecosystem productivity in a fluctuating environment: the insurance hypothesis. *Proceedings of the National Academy of Sciences* **96**, 1463-1468 (1999).
66. M. Galetti *et al.*, Ecological and evolutionary legacy of megafauna extinctions. *Biological Reviews* **93**, 845-862 (2018).
67. M. Davoli *et al.*, Megafauna diversity and functional declines in Europe from the Last Interglacial to the present. *Global Ecology and Biogeography* **33**, 34-47 (2024).
68. C. N. Johnson, Ecological consequences of Late Quaternary extinctions of megafauna. *Proceedings of the Royal Society B: Biological Sciences* **276**, 2509-2519 (2009).
69. J.-C. Svenning *et al.*, Science for a wilder Anthropocene: Synthesis and future directions for trophic rewilding research. *Proceedings of the National Academy of Sciences* **113**, 898-906 (2016).
70. A. Perino *et al.*, Rewilding complex ecosystems. *Science* **364**, eaav5570 (2019).
71. S. Hoeks *et al.*, Shifts in ecosystem equilibria following trophic rewilding. *Diversity and Distributions* **29**, 1512-1526 (2023).
72. T. N. Community, New and Old Worlds Database of Fossil Mammals (NOW). Licensed under CC BY 4.0. Release [September 2017], retrieved 5-2-2019 from (2019).
73. Anonymous (2019) The Paleobiology Database. (https://paleobiodb.org).
74. J. L. Cantalapiedra *et al.*, The rise and fall of proboscidean ecological diversity. *Nature Ecology & Evolution* **5**, 1266-1272 (2021).
75. K. M. Cohen, S. C. Finney, P. L. Gibbard, J.-X. Fan, The ICS international chronostratigraphic chart. *Episodes* **36**, 199-204 (2021).
76. I. Žliobaitė *et al.*, Herbivore teeth predict climatic limits in Kenyan ecosystems. *Proceedings of the National Academy of Sciences* **113**, 12751-12756 (2016).
77. M. Fortelius *et al.*, An ecometric analysis of the fossil mammal record of the Turkana Basin. *Philosophical Transactions of the Royal Society B: Biological Sciences* **371**, 20150232 (2016).
78. I. Zliobaite *et al.*, Dental ecometrics of tropical Africa: linking vegetation types and communities of large plant-eating mammals. *Evolutionary Ecology Research* **19**, 127-147 (2018).
79. P. Andrews, J. Lord, E. M. N. Evans, Patterns of ecological diversity in fossil and modern mammalian faunas. *Biological Journal of the Linnean Society* **11**, 177-205 (1979).
80. M. Hernández Fernández, Rodent paleofaunas as indicators of climatic change in Europe during the last 125,000 years. *Quaternary Research* **65**, 308-323 (2006).
81. M. Chen, C. A. Strömberg, G. P. Wilson, Assembly of modern mammal community structure driven by Late Cretaceous dental evolution, rise of flowering plants, and dinosaur demise. *Proceedings of the National Academy of Sciences* **116**, 9931-9940 (2019).
82. R Development Core team, R: A language and environment for statistical computing. *R Foundation for Statistical Computing. Vienna, Austria. Internet: http://www.R-project.org* (2013).
83. D. Mouillot *et al.*, Functional over-redundancy and high functional vulnerability in global fish faunas on tropical reefs. *Proceedings of the National Academy of Sciences* **111**, 13757-13762 (2014).
84. A. D. Muscente *et al.*, Ediacaran biozones identified with network analysis provide evidence for pulsed extinctions of early complex life. *Nature Communications* **10**, 911 (2019).
85. A. D. Muscente *et al.*, Quantifying ecological impacts of mass extinctions with network analysis of fossil communities. *Proceedings of the National Academy of Sciences* **115**, 5217-5222 (2018).
86. D. Edler, M. Rosvall (2015) The infomap software package. (See http://www.mapequation.org).
87. M. Rosvall, C. T. Bergstrom, Maps of random walks on complex networks reveal community structure. *Proceedings of the National Academy of Sciences* **105**, 1118-1123 (2008).
88. R. Bernardo-Madrid *et al.*, Human activity is altering the world's zoogeographical regions. *Ecology letters* **22**, 1297-1305 (2019).
89. J. Rissanen, Modeling by shortest data description. *Automatica* **14**, 465-471 (1978).
90. A. Lancichinetti, S. Fortunato, Community detection algorithms: a comparative analysis. *Physical review E* **80**, 056117 (2009).
91. A. Baselga, C. D. L. Orme, betapart: an R package for the study of beta diversity. *Methods in ecology and evolution* **3**, 808-812 (2012).

Suppementary Information

Material and methods

Network Analysis

Functional assembly vs. taxonomical assembly. In order to compare the dynamics of community assembly processes at functional and taxonomic levels, we built the taxonomical version of the described dataset for functional types. By doing so, we obtained the same continent-stage as for the functional dataset, 3046 species in 78 continent-stage (Fig. S1).

Node characterization. We also characterized the importance of the nodes (i.e. functional types/taxa and continent-stage) in the definition of particular modules. To do so, we used the IndVal index (1, 2) that considers the affinity and fidelity of a node to the module where it was classified. The affinity of a node, *Ai*, is calculated as the number of links to nodes classified in its same module, *Xi*, relative to the total number of nodes in the module, *Z*,

$Ai = Xi/Z$ (Eq. 1)

For instance, a functional type (or taxa) occurring in a large proportion of continent-stage within the same module will show a high affinity for it. On the other hand, the fidelity, *Fi*, of a node is defined by the number of links inside its module, *Ni*, compared to its total number of links, *L*,

$Fi = Ni/L$ (Eq. 2)

For instance, a species only occurring in the continent-stage of its own module will have a high-fidelity value to it. IndVal index is calculated as $IndVal = Ai \times Fi$. Thus, a node that links to most of the nodes of its own module (high affinity) and is not connected to nodes in other modules (high fidelity) will show a high IndVal.

Module characterization

We calculated the IndVal index to study the importance of the nodes in the definition of their modules. Here, we used this index to extract the most singular FTs in the modules. Through a 0.95 quantile, we extracted these singular FTs for each module. Then, we look inside these FTs to study the most abundant trait states in their species composition functional traits pool (Fig. S4 to S17).

The taxonomic composition of the modules can give us information about their structure and how the changes in this composition influenced the module shifts. To explore this, we calculated the relative abundance of the families that compose the species pool of these high IndVal FTs for each module (Fig. S18).

Linear models of functional diversity

In order to correct for the sampling effect of the differential number of occurrences in the different continent-stage (3, 4), We extracted the residuals from the linear models over the indexes results (5). First, we fitted linear models where functional diversity is a function of the number of occurrences while allowing the relationship to change among continents (index ~ occurrences*continent). Second, we fitted linear models where functional diversity is a function of the number of occurrences and the quadratic of this number (index ~ occurrences*occurrences^2). To decide which model corrects better for the sampling effect on the differential occurrence number,

we used the Akaike's information criterion corrected for small sample size (AICc). Following Blanco*, et al.* (6), we assumed a difference of two AICc units to consider that two models are significantly different. If two models were equivalent based on AICc we chose the one with fewer parameters as a rule of parsimony. For the three indexes (Shannon, Evenness and Richness), the occurrences*continent model resulted in the best model, and we used the residuals from it for the subsequent analysis (Table S2).

Moments of abrupt physical and environmental change have been linked to reorganizations of functional structure (6). To explore this, we fitted linear models using the corrected functional diversity indexes (see above) as a function of the continent-stage age as an explanatory variable (corrected index ~ age). We used the function *segmented* in *R* to look for the breakpoints in the residuals of the linear model. We plotted along with the corrected index evolution through time (Fig. 2). Besides, to see how the functional diversity trends affected at geographical level and functional structure, we plotted the residuals indexes by continents through time (Fig. 2B).

Functional distance among continents over time

In order to identify functional resemblance among continents over time, we calculated the functional distances as the distance of the continent-stage in the functional dissimilarity space. We plotted the resulting measure over time using continent pairs (Fig. S3).

Sensitivity analysis

Sensitivity analysis on the k-means groups. We tested the selection criterion of 406 FT based on the number of unique combinations of functional traits. We ran the k-means analysis selecting 100, 200, 300, 400 and 500 groups, and we repeated 100 times. We used this to build the analysis database and run infomap following the above explained procedure. As a result, we plotted the quality code length (measure of modularity) and the number of modules obtained from the network analysis for all k-means randomization (Fig. S19). In both cases the variable values become stable around 400 FT.

Sensitivity analysis to sampling. When working with paleontological data, we should always be aware of potential sampling biases that could drastically affect the results of our analyses (i.e. some epochs being better sampled, countries or regions with difficult access to conduct fieldwork, historical preferences…). In other words, the disparate number of species across the analyzed bins could impact the estimated functional similarity between them. To test this, we conducted a sensitivity analysis where we performed a rarefaction procedure (3, 4) on the species present in each continent-stage. We randomly selected 20 species from each bin, and then we ran the network and beta diversity analysis (see above for detailed explanation) on the rarefied dataset. We repeated the procedure 100 times. An averaged distance matrix from the 100 draws was used to estimate functional turnover between bins and to compare with our main results (Fig. S20). The results from the rarefactions were highly congruent with those derived from the full dataset.

Sensitivity analysis to the effect of aggregation. We tested whether the emerging pattern of our functional structure analyses could be just a byproduct of merging species into functional types. To do so, we compared the modularity of observed functional networks against that of null networks where the species were randomly classified into functional types, keeping constant the number of species belonging to each functional type. To calculate the network's modularity using the Infomap framework, we computed a relative code length by dividing the code length of the network with modules by the code length of the network without modules. When the network lacks a modular

structure the index equals 1, whereas it approaches 0 for highly modular networks. To make the index increase with network modularity, we computed the complement of the relative code length,

$M = 1 - CLm/CL$ (Eq. 3)

where CLm represents the code length of the network with modules and CL the code length of the network without modules. Finally, we calculated the p-value of the observed network being more modular than random expectations as the proportion of 100 null networks plus the observed one being more modular than or equal to the observed network (Fig. S21).

Sensitivity analysis to community detection. We identified two principal sources of uncertainty regarding the detection of network modules. Firstly, several community detection algorithms (Infomap included) use stochastic searches to find optimal network partitions. The most common procedure is to run the algorithm an elevated number of times and pick the best quality partition. This, however, brings questions on the number of runs needed to avoid local optima (i.e. obtaining a complete solution landscape) and the consistency of modules across runs of similar quality (7). To approach the first issue, we used a 10-fold cross validation exploring the probability that a test partition has a similarity higher than 0.75 to one of the training partitions (7). We found that 10,000 Infomap runs provided a complete solution landscape with ~1 probability for a test partition being more similar than 0.75 to training partitions, both for the functional and taxonomic networks. To handle the second issue, we explored whether the modules of the best network partition were consistent across the remaining 9,999 partitions. For a given module, we computed the probability of finding a module with similarity higher than a given threshold in the remaining partitions (7). We used a similarity threshold of 0.5 (which implies a one-to-one correspondence) and a more conservative threshold of 0.75. Regardless of the threshold, the modules obtained in the best partitions were highly consistent across different solutions; they showed probabilities 1 of being obtained in different solutions (Fig. 1, Table S2).

Sensitivity analysis to accuracy of network partition vs functional distances. We ran a Permutational multivariate analysis of variance (PERMANOVA) to test whether the module partition from network analysis reflects the functional distances between the continent-stage. We obtained that the module partition is similar to functional distances by a statistically significant $p>0.001$.

We used *R* software (8) for all the analyses. All the scripts and database used are at: https://github.com/f-blanco/ecoherb

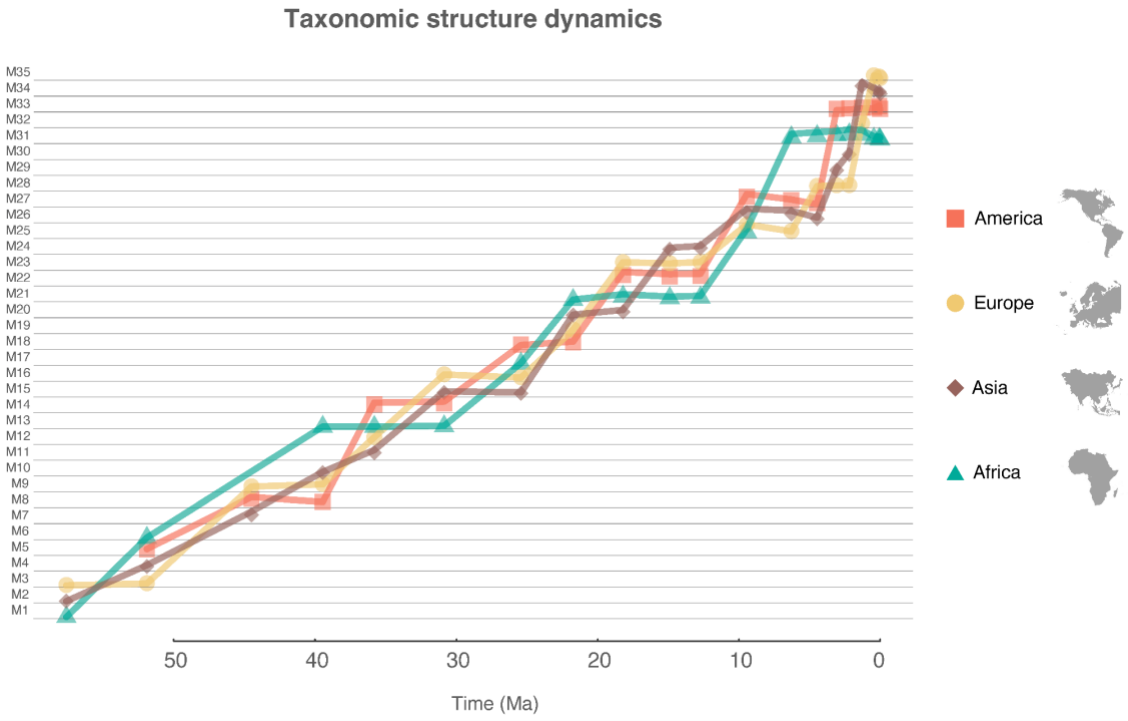

Fig. S1. Large herbivore´ taxonomic structure dynamics. Taxonomic structure trends in the different continents are plotted by colors against time in Myrs. Shapes indicate time bins in each continent. Modules (M) derived from network analysis show the functional structure succession in each continent.

Fig. S2. Beta diversity evolution over the Cenozoic. Evolution of the beta diversity and its components (nestedness and turnover) are plotted by colors against time in Myrs for each continent.

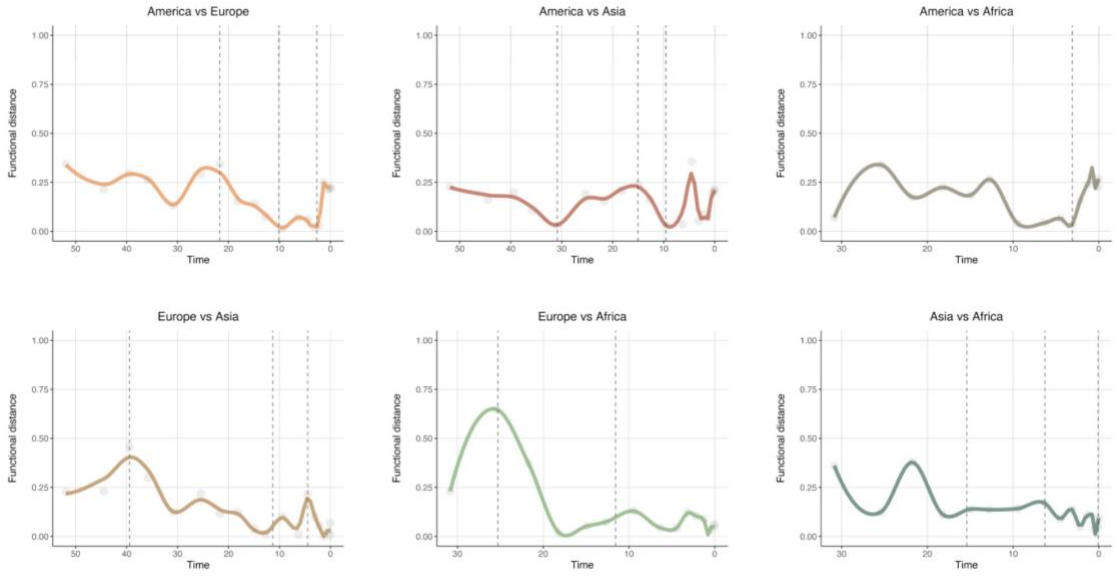

Fig. S3. Continents' functional distance through time. Functional distance between continent pairs calculated from the functional space in Fig. 1B is plotted against time in myr**.** Line colors are derived from the combination of continent color in Fig. 1A. Dotted lines are inflection points from regression models with segmented relationships (see methods).

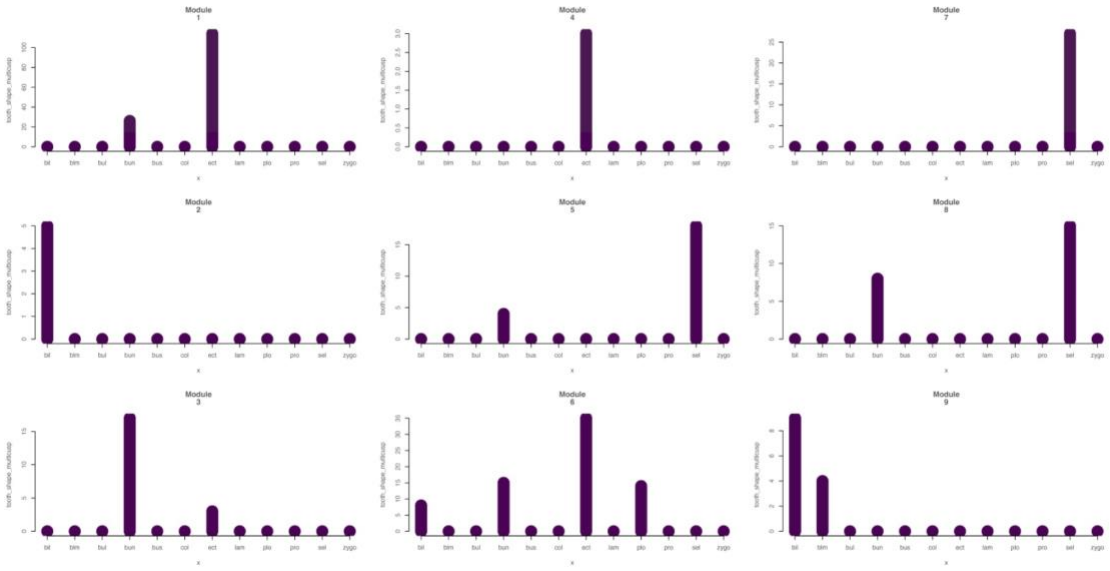

Fig. S4. Most abundant trait states by module. Traits state abundance are calculated for the traits of significant higher IndVal values (see methods) in each module. X axis represents the different states corresponding to the trait.

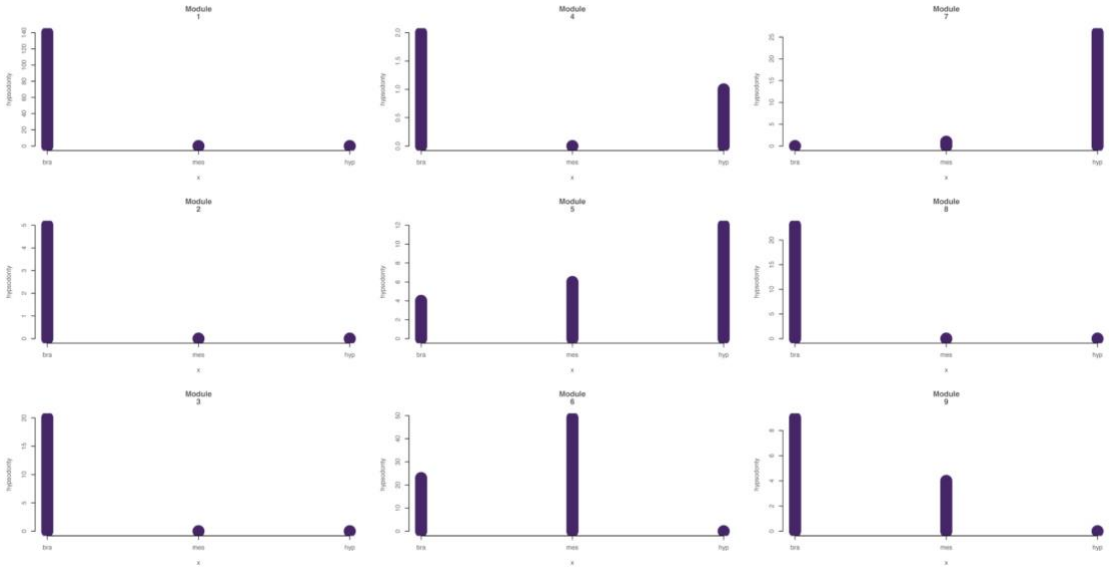

Fig. S5. Most abundant trait states by module. Traits state abundance are calculated for the traits of significant higher IndVal values (see methods) in each module. X axis represents the different states corresponding to the trait.

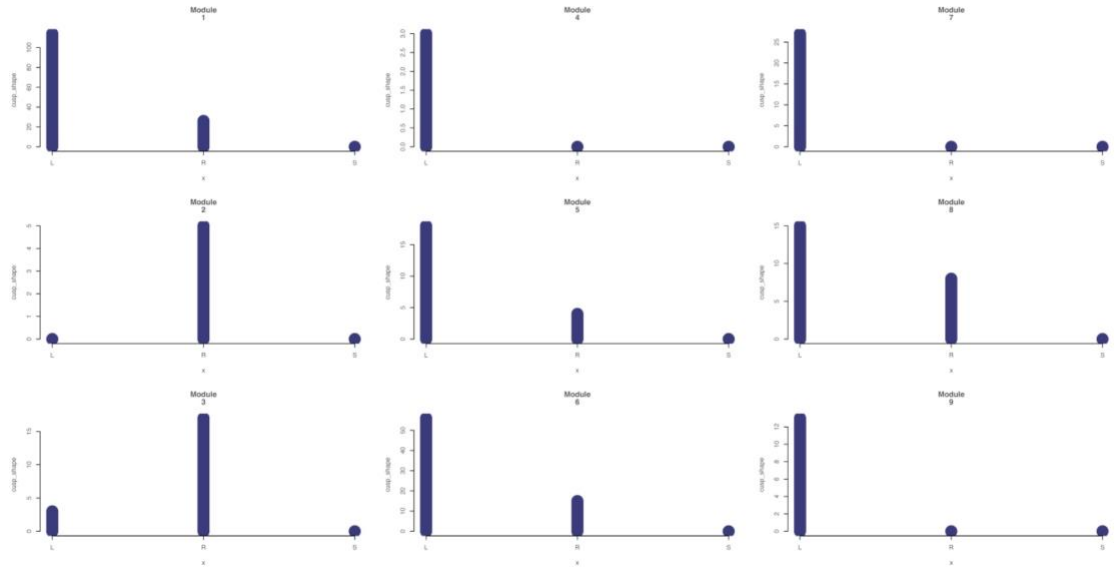

Fig. S6. Most abundant trait states by module. Traits state abundance are calculated for the traits of significant higher IndVal values (see methods) in each module. X axis represents the different states corresponding to the trait.

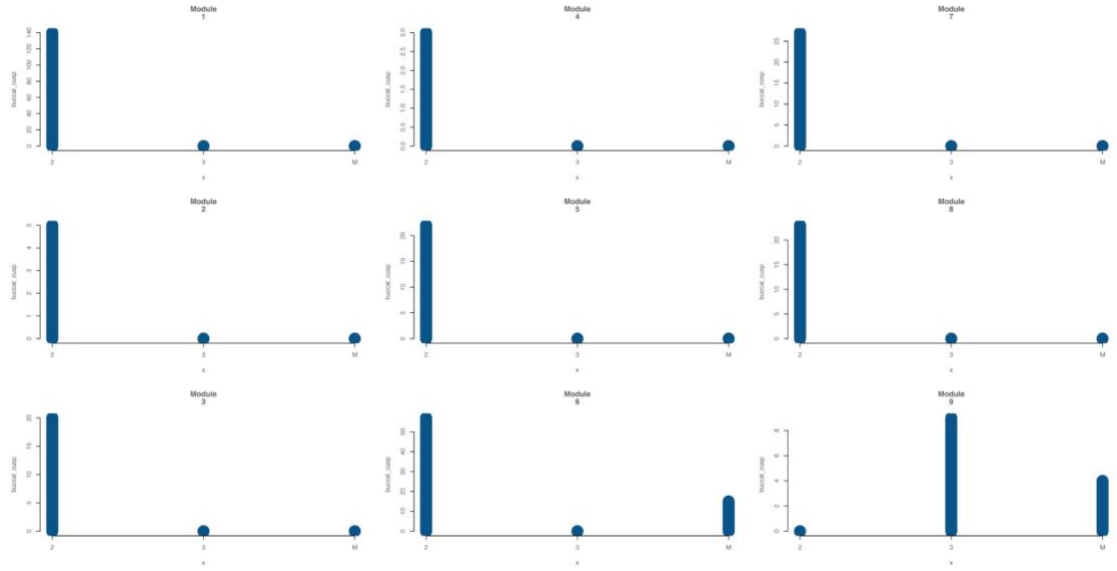

Fig. S7. Most abundant trait states by module. Traits state abundance are calculated for the traits of significant higher IndVal values (see methods) in each module. X axis represents the different states corresponding to the trait.

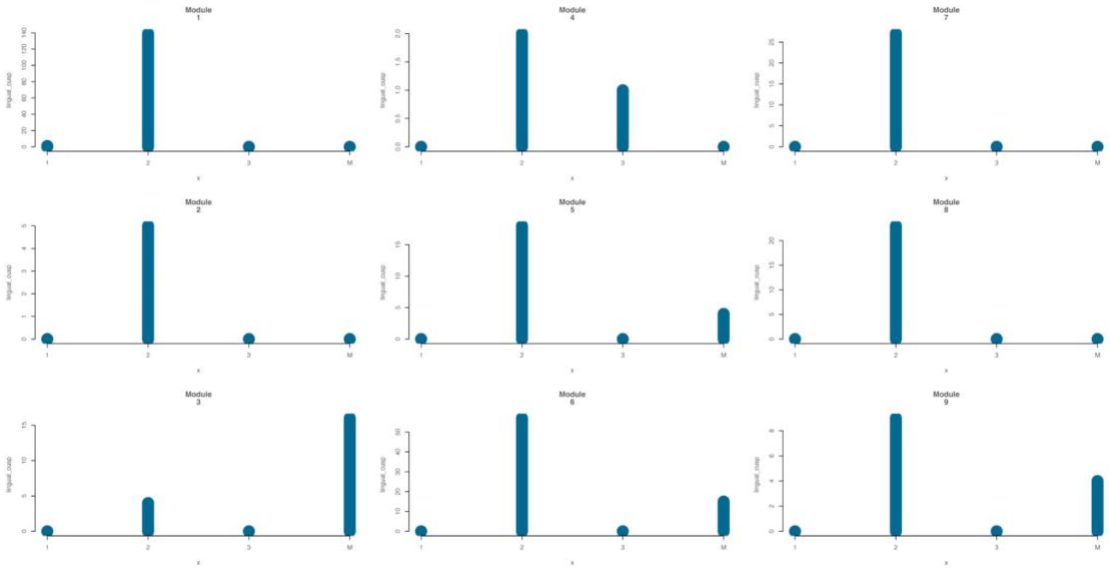

Fig. S8. Most abundant trait states by module. Traits state abundance are calculated for the traits of significant higher IndVal values (see methods) in each module. X axis represents the different states corresponding to the trait.

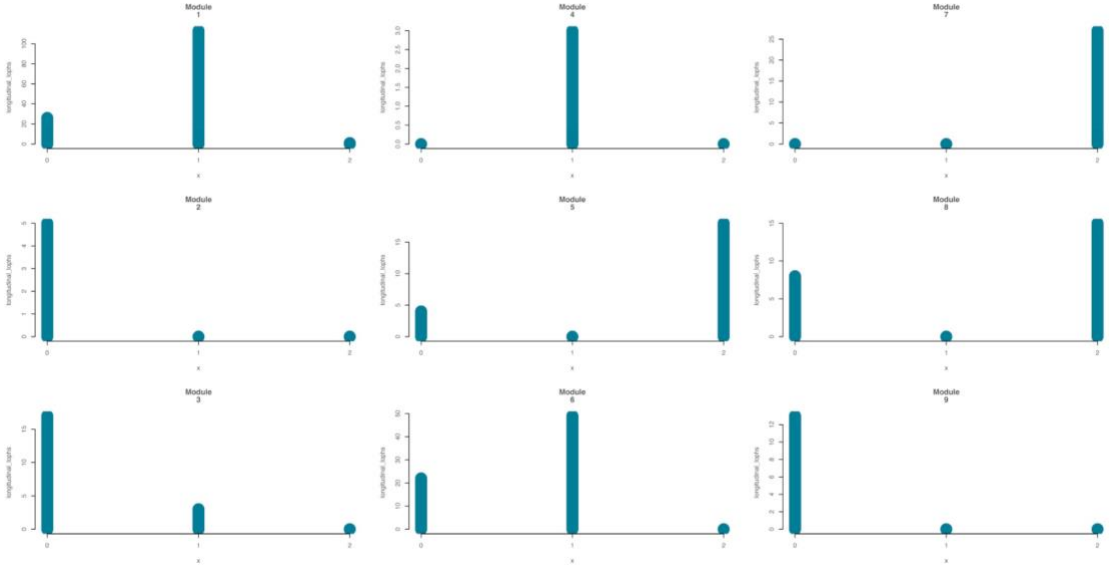

Fig. S9. Most abundant trait states by module. Traits state abundance are calculated for the traits of significant higher IndVal values (see methods) in each module. X axis represents the different states corresponding to the trait.

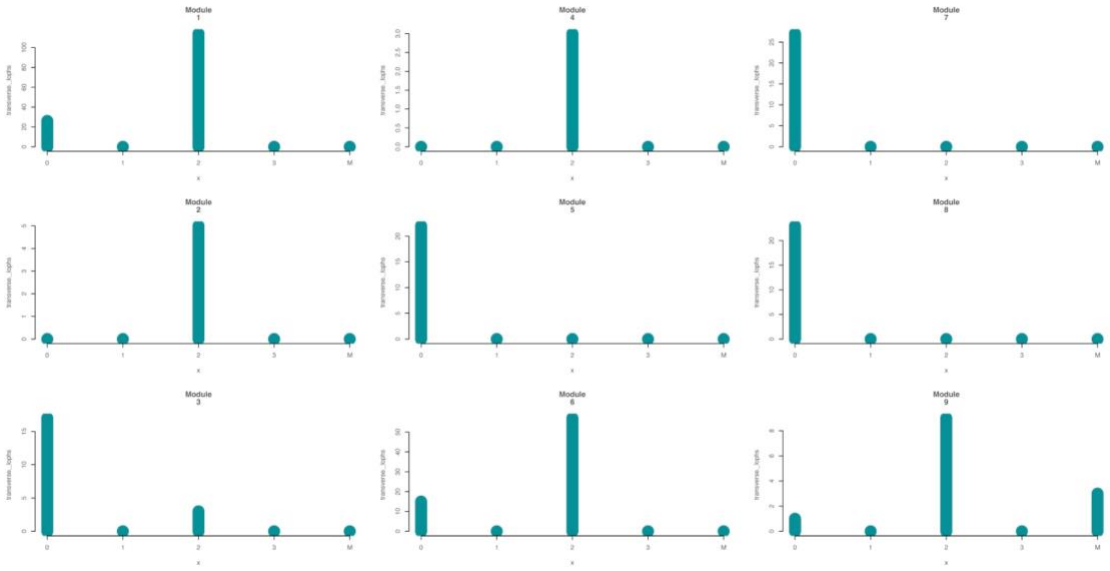

Fig. S10. Most abundant trait states by module. Traits state abundance are calculated for the traits of significant higher IndVal values (see methods) in each module. X axis represents the different states corresponding to the trait.

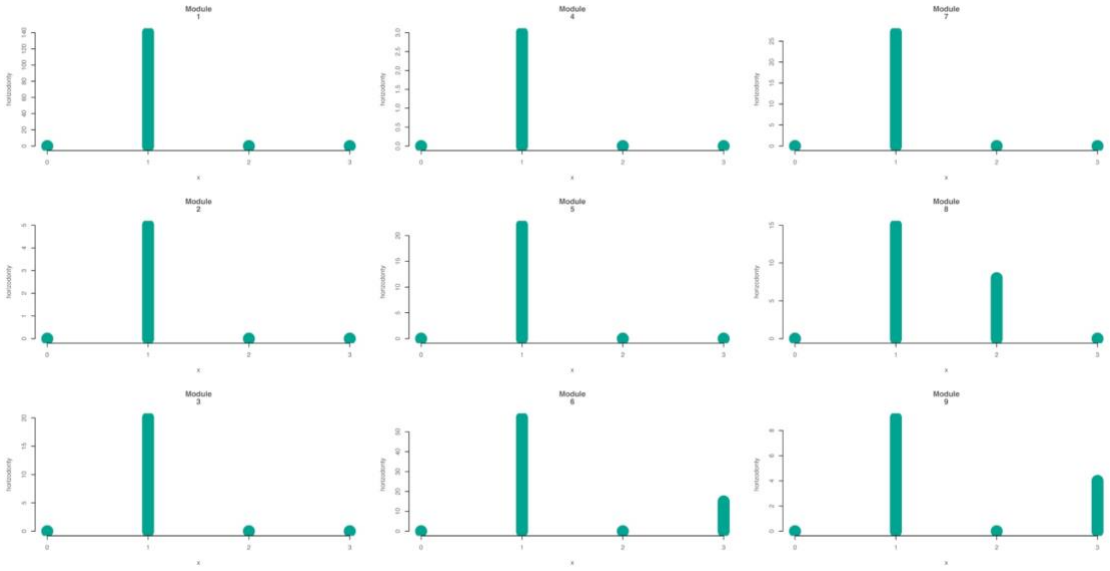

Fig. S11. Most abundant trait states by module. Traits state abundance are calculated for the traits of significant higher IndVal values (see methods) in each module. X axis represents the different states corresponding to the trait.

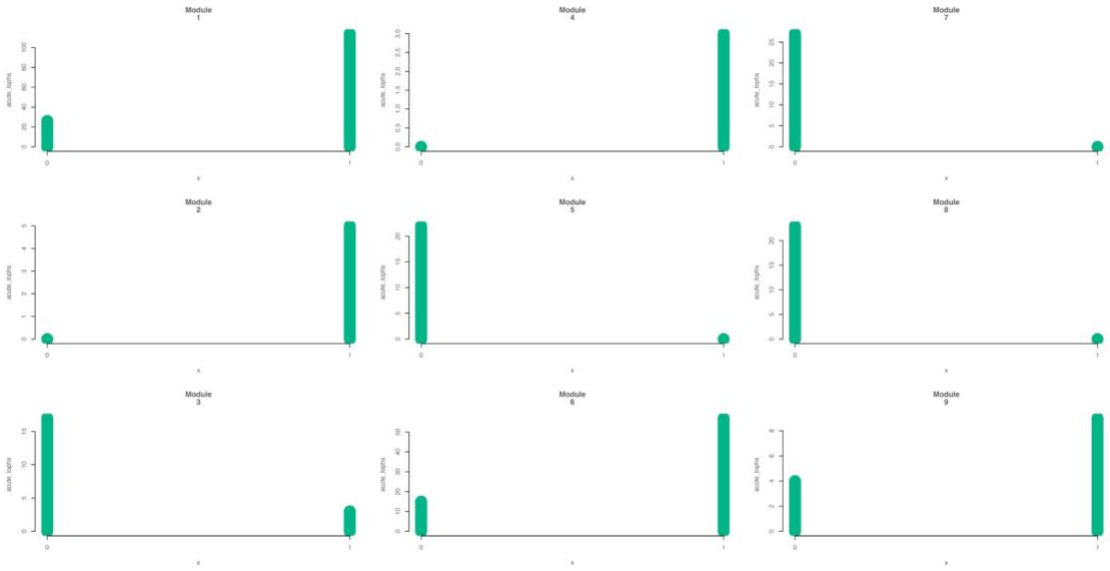

Fig. S12. Most abundant trait states by module. Traits state abundance are calculated for the traits of significant higher IndVal values (see methods) in each module. X axis represents the different states corresponding to the trait.

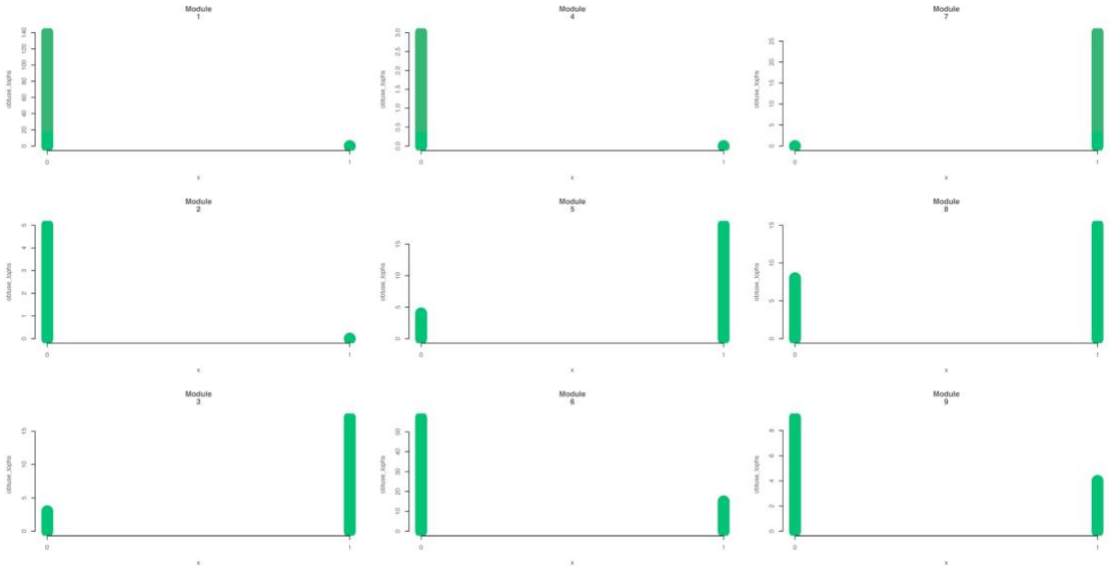

Fig. S13. Most abundant trait states by module. Traits state abundance are calculated for the traits of significant higher IndVal values (see methods) in each module. X axis represents the different states corresponding to the trait.

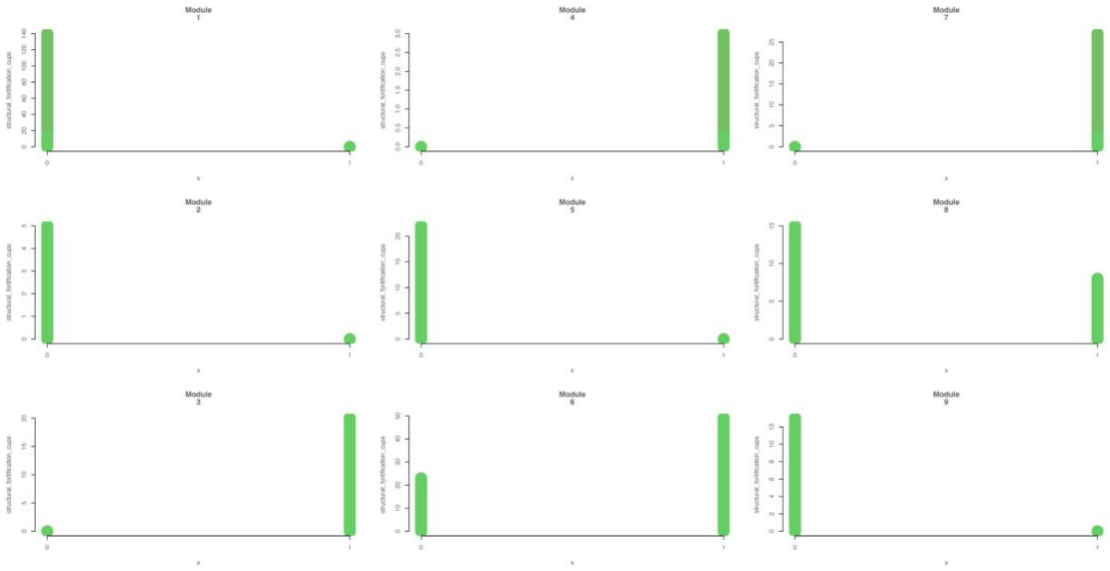

Fig. S14. Most abundant trait states by module. Traits state abundance are calculated for the traits of significant higher IndVal values (see methods) in each module. X axis represents the different states corresponding to the trait.

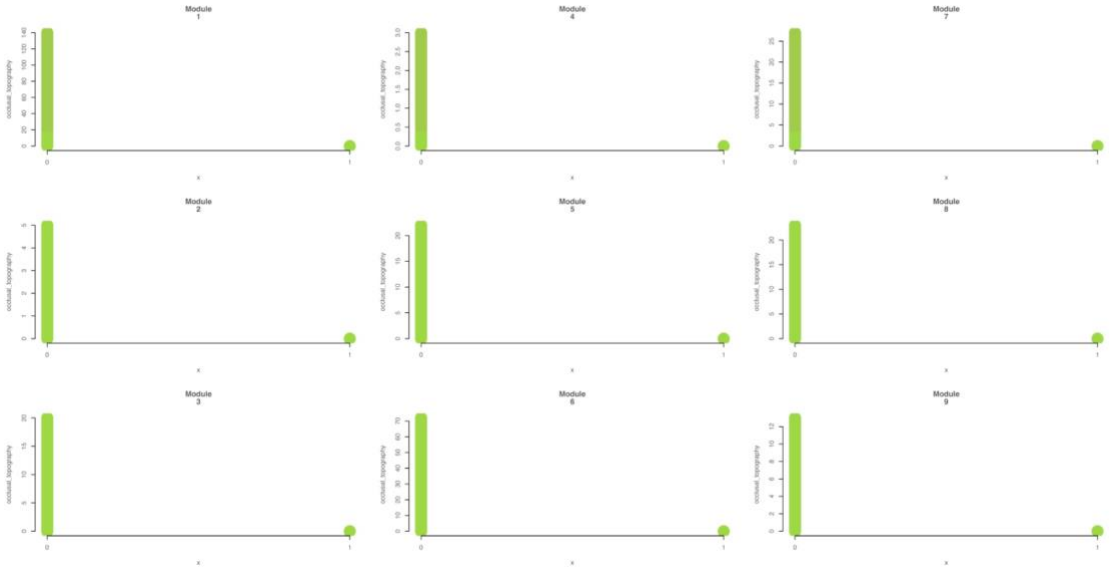

Fig. S15. Most abundant trait states by module. Traits state abundance are calculated for the traits of significant higher IndVal values (see methods) in each module. X axis represents the different states corresponding to the trait.

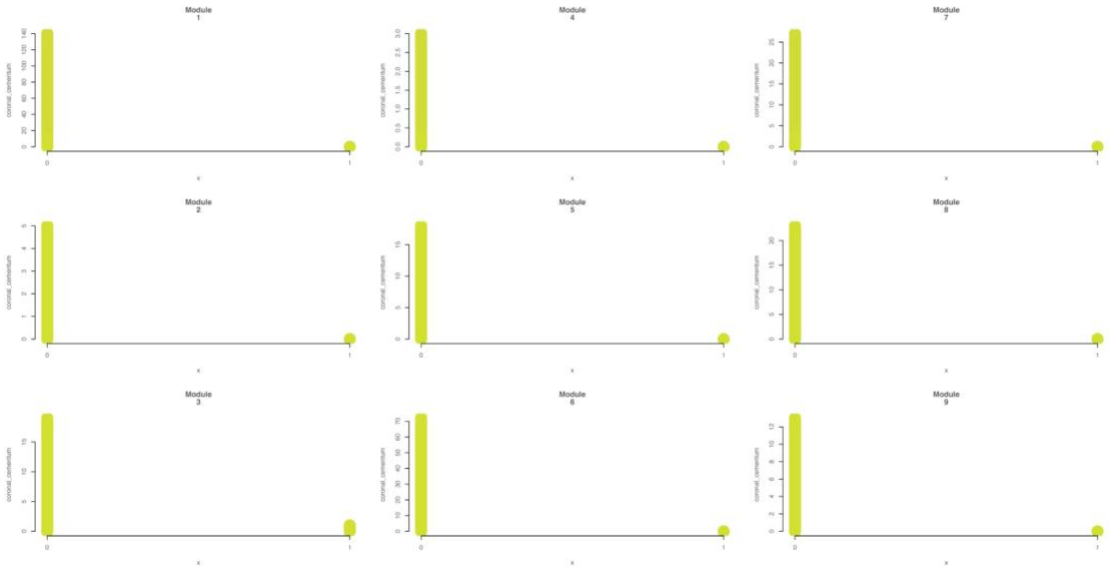

Fig. S16. Most abundant trait states by module. Traits state abundance are calculated for the traits of significant higher IndVal values (see methods) in each module. X axis represents the different states corresponding to the trait.

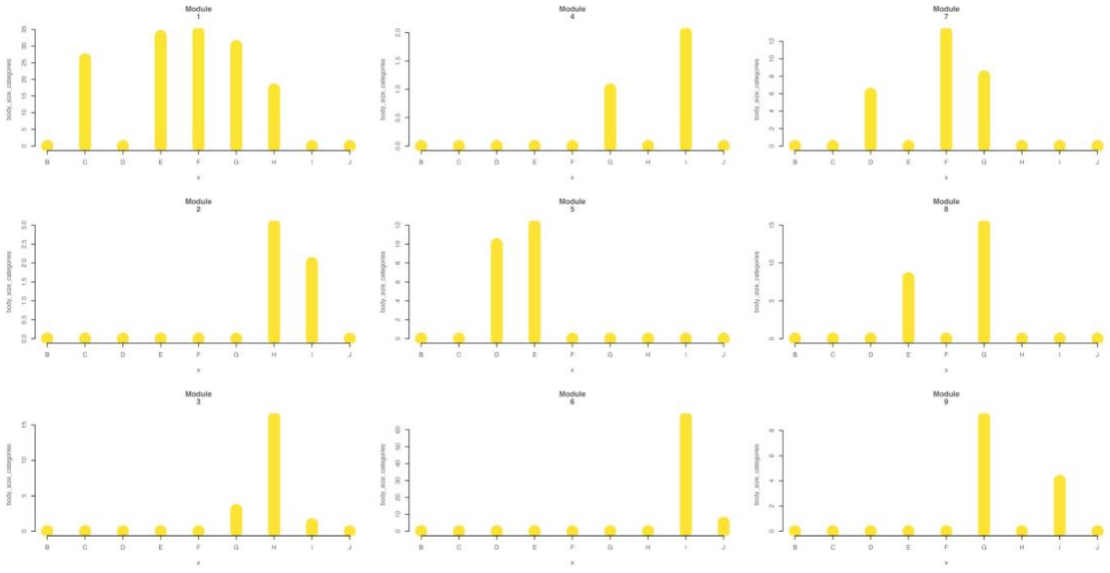

Fig. S17. Most abundant trait states by module. Traits state abundance are calculated for the traits of significant higher IndVal values (see methods) in each module. X axis represents the different states corresponding to the trait.

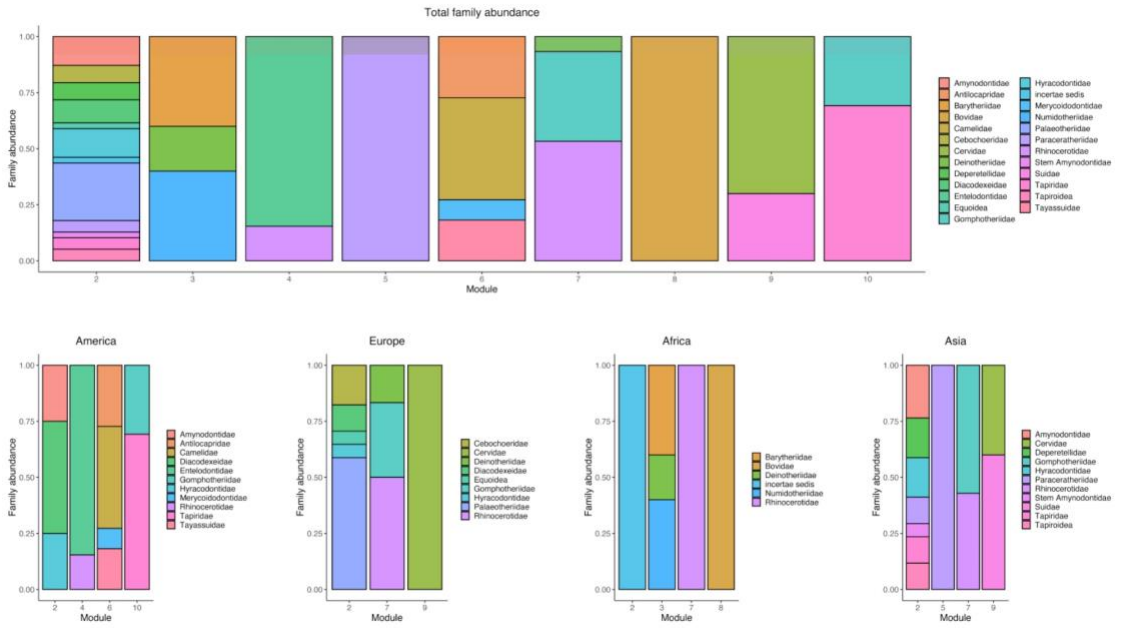

Fig. S18. Family abundance by module. Family abundances in total (above) and by continent (below), are calculated using only the ones with higher IndVal values for each module (see methods). Colors represent the different families present in each module.

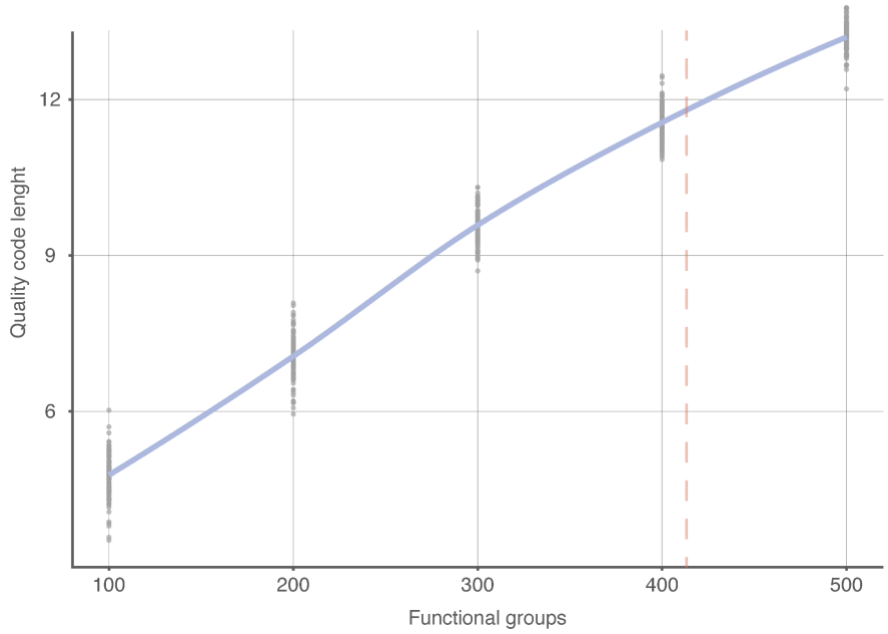

Fig. S19. K-means sensitivity analysis. Quality code length (measure of modularity) is plotted against the number of modules obtained from the network analysis for all k-means randomization (see methods). Dashed red line represents the number of modules used for the analysis (405).

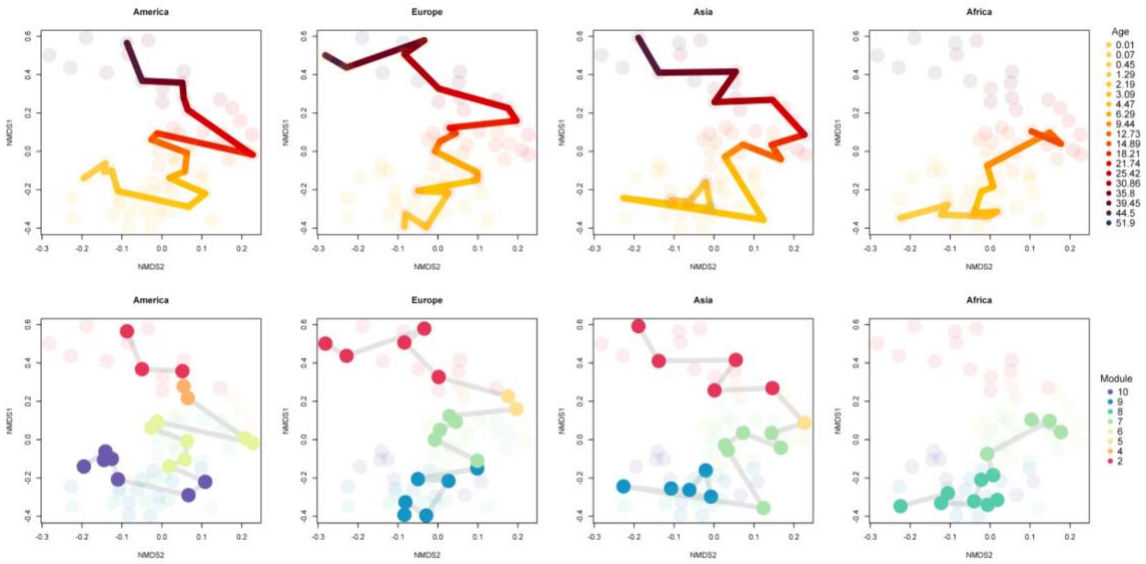

Fig. S20. Randomized results of functional structure. Functional space for each continent from time bin functional distances calculated as turnover plotted in two dimensions through NMDS (see methods). Dots represent functional time bins in each continent. Above color-scale indicates time in Myrs. Colors below represent the different modules from the network analysis (Fig. 1A).

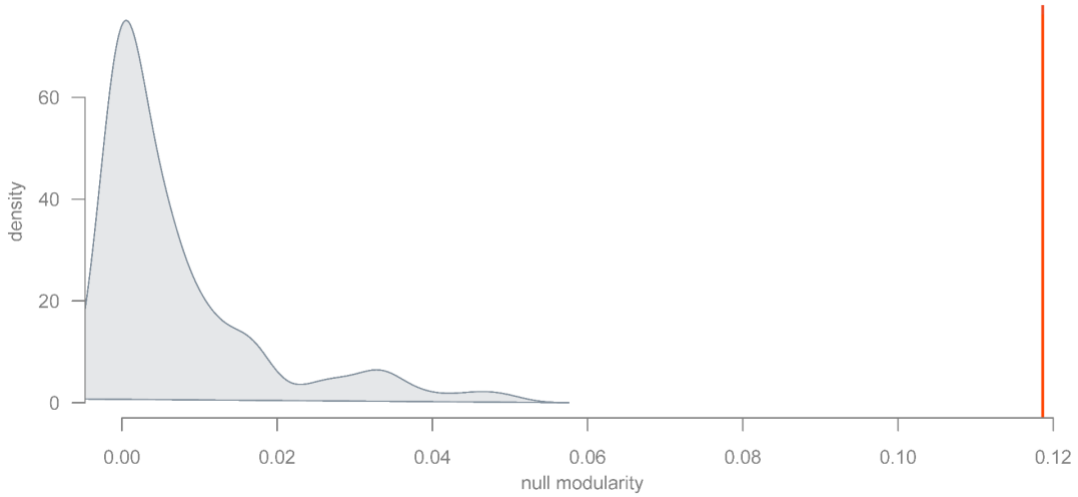

Fig. S21. Observed and simulated modularity of functional networks. Gray density diagrams show the modularity scores of 100 random networks compared with the observed network (red vertical line).

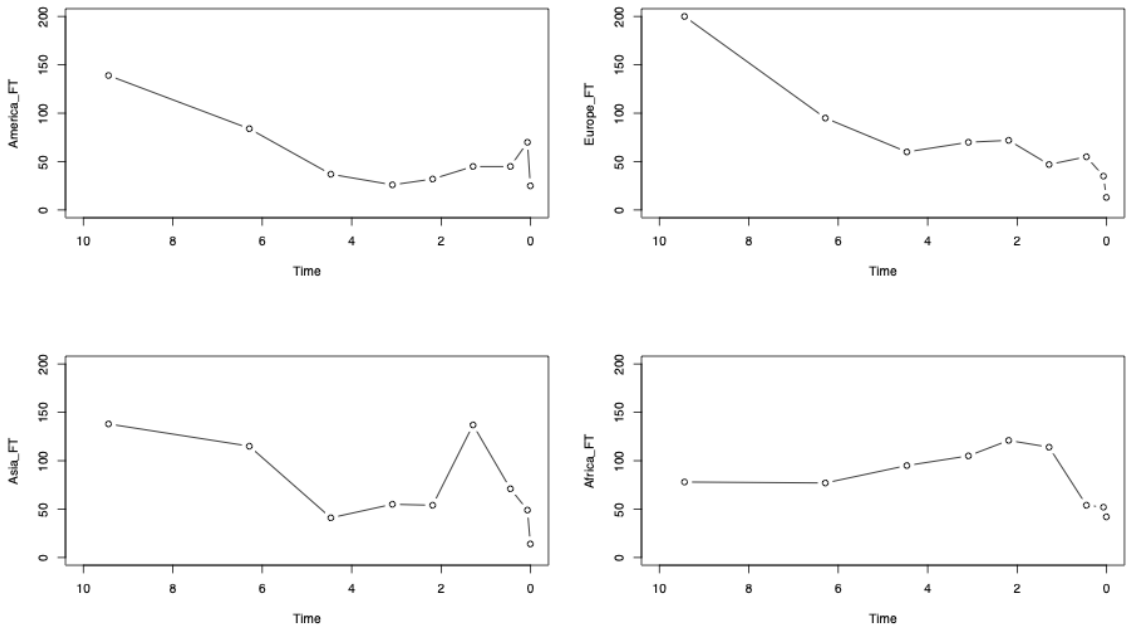

Fig. S22. Functional types evolution over the last 10 Ma. The total number of functional types by continent is plotted against time for the last 10Ma.

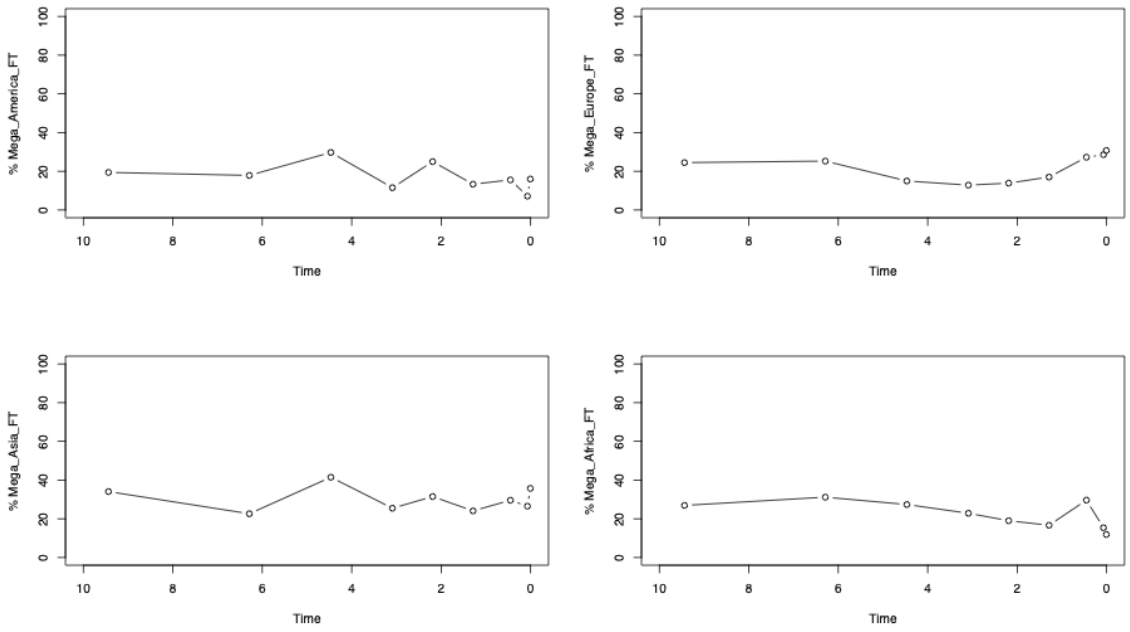

Fig. S23. Megafauna functional types evolution over the last 10 Ma. Percentage of the total functional types belonging to megafauna by continent is plotted against time for the last 10Ma.

Table S1. Probability of obtaining the same module partition with similarity >0.5 and >0.75 (Robustness) for the functional network.

Module	Robustness >0.5	Robustness >0.75
1	1	1
2	1	1
3	1	1
4	1	1
5	1	1
6	1	1
7	1	1
8	1	1
9	1	1

Table S2. Linear model comparison for functional diversity using occurrences*continent and occurrences*occurrences^2. K= number of estimated parameters in the model, AICc= Akaike information criterion , LL= log-likelihood.

M names	*K*	*AICc*	*Delta AICc*	*LL*
occurrences*continent	9	14.66	0.00	3.38
occurrences*occurrences^2.	5	39.68	25.22	-14.34

SI References

1. J.-M. Neuhaus, L. Sticher, F. Meins, Jr., T. Boller, A short C-terminal sequence is necessary and sufficient for the targeting of chitinases to the plant vacuole. *Proc. Natl. Acad. Sci. U.S.A.* 88, 10362–10366 (1991).
2. E. van Sebille, M. Doblin, Data from “Drift in ocean currents impacts intergenerational microbial exposure to temperature.” Figshare. Available at https://dx.doi.org/10.6084/m9.figshare.3178534.v2. Deposited 15 April 2016.
3. A. V. S. Hill, “HLA associations with malaria in Africa: Some implications for MHC evolution” in Molecular Evolution of the Major Histocompatibility Complex, J. Klein, D. Klein, Eds. (Springer, 1991), pp. 403–420.

1. R. Bernardo-Madrid *et al.*, Human activity is altering the world's zoogeographical regions. *Ecology letters* **22**, 1297-1305 (2019).
2. M. Dufrêne, P. Legendre, Species assemblages and indicator species: the need for a flexible asymmetrical approach. *Ecological monographs* **67**, 345-366 (1997).
3. D. M. Raup, Taxonomic diversity estimation using rarefaction. *Paleobiology* **1**, 333-342 (1975).
4. M. Foote, Rarefaction analysis of morphological and taxonomic diversity. *Paleobiology* **18**, 1-16 (1992).
5. D. M. Raup, Species diversity in the Phanerozoic: an interpretation. *Paleobiology* **2**, 289-297 (1976).
6. F. Blanco *et al.*, Punctuated ecological equilibrium in mammal communities over evolutionary time scales. *Science* **372**, 300-303 (2021).
7. J. Calatayud, R. Bernardo-Madrid, M. Neuman, A. Rojas, M. Rosvall, Exploring the solution landscape enables more reliable network community detection. *Physical Review E* **100**, 052308 (2019).
8. R Development Core team, R: A language and environment for statistical computing. *R Foundation for Statistical Computing. Vienna, Austria. Internet: http://www.R-project.org* (2013).